Progress in Oceanography 161 (2018) 47–65

Contents lists available at ScienceDirect

Progress in Oceanography

journal homepage: www.elsevier.com/locate/pocean

Habitat heterogeneity of hadal trenches: Considerations and implications for future studies

Heather A. Stewart[a,*], Alan J. Jamieson[b]

[a] British Geological Survey, Lyell Centre, Research Avenue South, Edinburgh EH14 4AP, UK
[b] School of Natural and Environmental Sciences, Newcastle University, Newcastle Upon Tyne NE1 7RU, UK

ARTICLE INFO

Keywords:
Bottom topography
Hadal zone
Ocean floor habitat
Oceanic trenches
Sediment distribution

ABSTRACT

The hadal zone largely comprises a series of subduction trenches that do not form part of the continental shelf-slope rise to abyssal plain continuum. Instead they form geographically isolated clusters of deep-sea (6000–11,000 m water depth) environments. There is a growing realization in hadal science that ecological patterns and processes are not driven solely by responses to hydrostatic pressure, with comparable levels of habitat heterogeneity as observed in other marine biozones. Furthermore, this heterogeneity can be expressed at multiple scales from inter-trench levels (degrees of geographical isolation, and biochemical province), to intra-trench levels (variation between trench flanks and axis), topographical features within the trench interior (sedimentary basins, ridges, escarpments, 'deeps', seamounts) to the substrate of the trench floor (seabed-sediment composition, mass movement deposits, bedrock outcrop). Using best available bathymetry data combined with the largest lander-derived imaging dataset that spans the full depth range of three hadal trenches (including adjacent slopes); the Mariana, Kermadec and New Hebrides trenches, the topographic variability, fine-scale habitat heterogeneity and distribution of seabed sediments of these three trenches have been assessed for the first time. As well as serving as the first descriptive study of habitat heterogeneity at hadal depths, this study also provides guidance for future hadal sampling campaigns taking into account geographic isolation, total trench particulate organic matter flux, maximum water depth and area.

1. Introduction

The hadal zone (water depths exceeding 6000 m) differs somewhat from shallower marine environments (littoral; < 200 m, bathyal; 200–2000 m and abyssal; 2000–6000 m; Gage and Tyler, 1991) because it is not a direct continuation of the preceding biozones *per se,* but rather the descending continuum from the coasts over the continental slopes and rises onto the abyssal plains eventually fragment into clusters of often vastly isolated hadal areas of varying size, depth, length, latitude and seismicity. These areas combined total over 800,000 km^{-2} and represents the deepest 45% of the global ocean (Jamieson et al., 2010). While the term 'hadal' refers to areas deeper than 6000 m (or 6500 m; Watling et al., 2013), this is largely a convenient nomenclature that does not reflect the complexity of habitats across the 5000 m depth range that it represents. The hadal zone is comprised largely of deep trenches formed by subduction at tectonic convergence zones, with additional representation in hadal troughs, which are non-seismic deep basins within abyssal plain interiors, and trench faults formed by the fracturing of mid-ocean ridge spreading centres perpendicular to the ridge axis. There are 27 subduction trenches, 13 troughs and seven trench faults (Jamieson, 2015); Table 1 and see supplementary material Fig. S1); i.e. 47 individual habitats between 6000 m and full ocean depth (10,984 m ± 25; Gardner et al., 2014).

The hadal frontier still challenges scientific endeavour as the great distances below the sea surface and immense hydrostatic pressure at depth has resulted in an almost notorious underrepresentation in marine science. In the pursuit of long-term sustainability of the oceans (Mengerink et al., 2014; Danovaro et al., 2017) it appears logical to treat the ocean in its entirety and not simply focus on the near and easily accessible areas. Although the last 10–15 years has seen a revival in hadal exploration, progress still lags behind that of coastal and inshore research (Jamieson and Fujii, 2011), and the diminishing grasp of biodiversity with increasing depth (Webb et al., 2010) is omnipresent despite the realisation that mankind is already impacting the deepest communities that we scarcely understand (Shimanaga and Yanagi, 2016; Jamieson et al., 2017). Furthermore, despite a range of diverse deep-sea technological capabilities that are now possible (Danovaro et al., 2014), full ocean depth rated instruments and vehicles are

* Corresponding author.
E-mail addresses: hast@bgs.ac.uk (H.A. Stewart), alan.jamieson@ncl.ac.uk (A.J. Jamieson).

https://doi.org/10.1016/j.pocean.2018.01.007
Received 26 August 2017; Received in revised form 9 November 2017; Accepted 16 January 2018
Available online 30 January 2018

relatively few in numbers (Jamieson, 2015; 2018).

Hadal biology and ecology has however progressed somewhat from simple cataloguing of species from great depths, as was the trend in the 1950s, to making the first attempts at ecological and evolutionary theory using large, statistically more robust data sets, and modern genetic and biochemical approaches (Yancey et al., 2014; Ritchie et al., 2015; Nunoura et al., 2015; Lacey et al., 2016; Tarn et al., 2016; Linley et al., 2017; Gerringer et al., 2017). Many of these studies are the first to pull comparative sampling from multiple trenches to challenge the idea that everything deeper that 6000 m is the same and any variation from abyssal communities is likely attributed to depth alone. However, as more sampling is undertaken there is a growing realisation that not everything is explained purely by pressure and in fact the habitats which support hadal fauna are as heterogenic as in any other marine biozone. Furthermore, this heterogeneity can be expressed at multiple scales from inter-trench levels (degrees of geographical isolation, and biochemical province), to intra-trench levels (variation in trench flanks and axis), topographical features within the trench interior (sedimentary ponds, ridges, escarpments, 'deeps', and seamounts) to the substrata of the trench floor (seabed sediment composition, mass movement deposits, bedrock outcrop).

In other more accessible marine habitats such as cold seeps (e.g. Levin et al., 2016), hydrothermal vents (e.g. Van Dover, 2000), submarine canyons (e.g. Amaro et al., 2016; Fernandez-Arcaya et al., 2017) and seamounts (e.g. Rowden et al., 2005), there is an established long-standing appreciation of the heterogeneity in substrata, structure, formation, connectivity and community composition, yet despite the hadal zone far exceeding these other environments in terms of depth range and footprint, virtually nothing is currently published on habitat heterogeneity on any scale smaller than inter-trench comparisons (and often only depth therein). This is in part due to so few exploratory vehicles having performed substantial seafloor imaging surveys, and those that have rarely publish. Science on the hadal frontier is therefore in a similar scenario to where more conventional deep-sea science was 50 or 60 years ago. However, a valuable resource that was capitalised on during that time is rarely found nowadays; publishing descriptive reports on images on the seafloor.

It was in the 1940s and 50s when underwater photography became an integral part of seafloor investigations (Ewing et al., 1946; Hahn, 1950; Emery, 1952; Pratt, 1962; Emery et al., 1965). The first scientifically useful images from hadal depths came from the Atlantic Ocean, in the Puerto-Rico and Romanche trenches (Pratt, 1962; Heezen et al., 1964; Heezen and Hollister, 1971), then from the South Sandwich Trench (Heezen and Johnson, 1965), and the New Britain and New Hebrides trenches (Heezen and Hollister, 1971). In 1962, ~4000 images of the hadal seafloor were taken by simple drop-cameras between 6758 and 8930 m on the American PROA expedition to the Palau, New Britain and New Hebrides trenches. Lemche et al. (1976) published the biological descriptions of these images in a well-illustrated report which is arguably still the best written reference as to what the hadal seafloor actually *looks* like, which is still an essential resource for scientists planning sampling campaigns to hadal trenches. These hard-won images provided the first glimpse at habitat heterogeneity in the hadal zone, but, unfortunately, after the 30 year hiatus in hadal exploration following the *Galathea, Vitjaz* and PROA expeditions to the introduction of the ROV *Kaikō*, the culture of publishing collections of seafloor images ceased. With the current lack of piloted vehicles operational at hadal depths, most studies rely on deploying free-fall systems and are thus jeopardising sampling success, quality of data interpretation and risk damage or loss of equipment by having literally no idea about the nature of the seafloor on which the equipment is to be deployed. In addition, cabled instruments are also easily damaged when deployed in unknown territory. Therefore any information of habitat heterogeneity at trench depths is invaluable in both the pursuit of establishing hadal ecological theory and in associated sampling operations.

This study serves as a review and reference guide for future hadal studies, taking into consideration greatly contrasting levels of hadal heterogeneity, ranging from geographic location and degrees of isolation between any given hadal zone and all others, through contrasting areas within a trench (adjacent flanks and trench axis) including complex topographical features within the trench interior. All to a backdrop of varying depths, sizes and food supply. All of these factors must be considered alongside the great water depths when planning research and interpreting results. We also report on the largest lander-derived imaging dataset that spans the full depth range of three hadal trenches (including adjacent slopes); the Mariana, Kermadec and New Hebrides trenches (Fig. 1). While the images were taken (and published) for biological and ecological studies, each deployment photographed or filmed an area of seafloor with often highly contrasting or surprising results, and therefore would serve as a crude seafloor survey of a largely inaccessible ecosystem on which to provide some guidance for current or forthcoming sampling campaigns at similar depths. This analysis also serves as the first descriptive documentation of habitat heterogeneity at hadal depths as the nature of the seafloor substratum has a profound effect on the composition of the benthic communities and biogeochemical processes (Thistle, 2003).

2. Materials and methods

2.1. Location and isolation of hadal zones

The analysis of broadscale trench topography was undertaken in ArcGIS. The trench boundaries were selected manually across contours superimposed on bathymetry of the trench derived from the General Bathymetric Chart of the Oceans (GEBCO www.gebco.net). The maps were projected to the cylindrical equal area projection with a central meridian 180° and a standard parallel 30° S, with a sub-kilometre spatial resolution. The location of each trench was identified using the position of the deepest point (Table 1). The topographic analysis was focussed further by slicing the bathymetry into 500 m depth bins. This approach also permitted the extraction of habitat size (km^{-2}) with depth.

To provide a measure for trench isolation, a geographic distance matrix was calculated in kilometres, for each point, for all pairwise combinations, from a database of deepest points of the 47 hadal zones between 6000 m water depth and full ocean depth. The Geographic Distance Matrix Generator used the semi-major axis of the WGS84 reference system as the default radius of the earth (Ersts [Internet]).

All statistical analysis was produced using R (R Development Core Team, 2005), figures were produced using ggplot2 (Wickham and Chang, 2007). The relationships between how isolated hadal zones are geographically from every other hadal zone was examined by first undertaking K-means clustering using euclidian distance and average linkage which revealed that a five cluster solution was best for determining a value of 'isolation' using the distance matrix data. This information was used in hierarchical agglomerative cluster analysis with bootstrapped p-values to determine whether the clusters were strongly supported by the data. Four of the clusters have a confidence of ≥80% with a confidence value of 67% assigned to the final cluster.

2.2. The study areas

The Kermadec Trench is formed by the subduction of the Pacific Plate below the Australian Plate resulting in a trench 1500 km in length and 60 km wide on average (Angel, 1982); Fig. 1B). The trench forms a

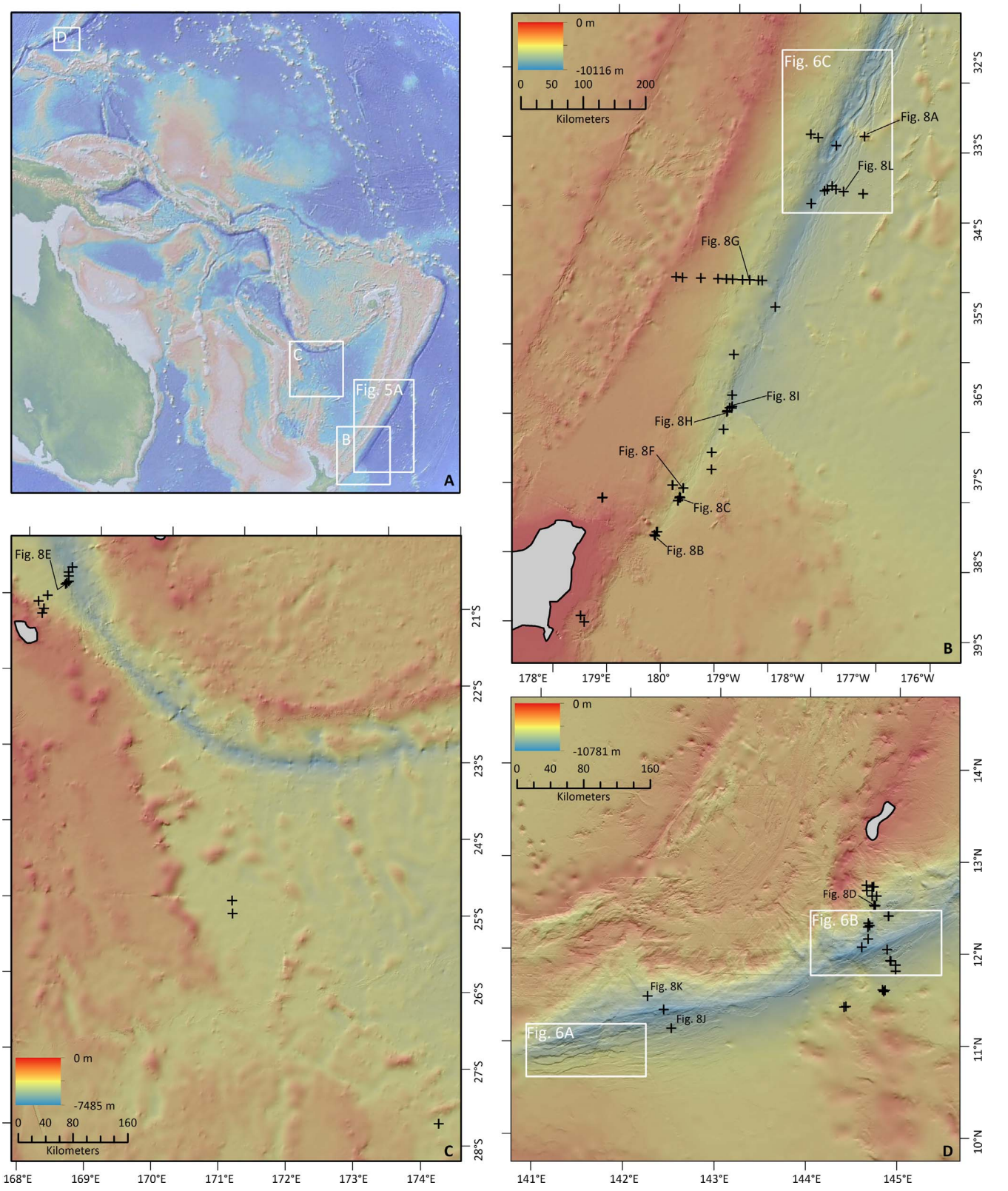

Fig. 1. Overview of the western Pacific Ocean study area (A) showing location of the study areas within the Mariana, Kermadec and New Hebrides trenches and the South Fiji Basin (adapted from Google Earth, Google 2017). Abyssal-lander and Hadal-lander deployments (black crosses) within the Kermadec Trench (B), the New Hebrides Trench and South Fiji Basin (C), and the Mariana Trench (D). All bathymetry sourced from the Global Multi-Resolution Topography (GMRT) Synthesis (Ryan et al. 2009).

continuum with the Tonga Trench immediately to the north and separated from the Kermadec Trench at the intersection of the Louisville Seamount Chain at approximately 25°40′S where water depths shallow to around 5100 m on the seamount and around 5600 m along the trench axis. The Kermadec Trench attains a maximum depth of 10,177 m at the 'Scholl Deep' and is oriented roughly north-northeast–south-southwest. The New Hebrides Trench is located to the northwest of the Kermadec, east of New Caledonia and attains a maximum depth of 7156 m and is

Table 1
List of 27 subduction trenches, 13 troughs and seven trench faults between 6000 m water depth and full ocean depth (adapted from Jamieson 2015). The maximum depth of each hadal area is derived from the General Bathymetric Chart of the Oceans (GEBCO www.gebco.net). Updated depths from recent studies: [*]Jamieson et al., 2011; [**]Gardner et al., 2014; [***]Wenzhöfer et al., 2016, [****]Personal observation, A.J. Jamieson.

Trenches	Ocean	Latitude	Longitude	Max depth (m)
Admiralty	Pacific	00.5600° S	149.3800° E	6887
Aleutian	Pacific	50.8791° N	173.4588° W	7669
Atacama	Pacific	23.3679° S	71.3473° W	8074[*]
Banda	Pacific	05.3852° S	130.9175° E	7329
Bougainville	Pacific	06.4762° S	153.9323° E	9103
Hjort	Pacific	58.4400° S	157.6800° E	6727
Izu-Bonin	Pacific	29.8038° N	142.6405° E	9701
Japan	Pacific	36.0800° N	142.7500° E	8412
Java	Indian	11.1710° S	118.4669° E	7290
Kermadec	Pacific	31.9270° S	177.3126° W	10,177
Kurile-Kamchatka	Pacific	44.0700° N	150.1800°E	10,542
Mariana	Pacific	11.3808° N	142.4249° E	10,984[**]
Middle America	Pacific	13.9097° N	93.4728° W	6547
New Britain	Pacific	07.0225° S	149.1623° E	8844
New Hebrides	Pacific	23.0733° S	172.1502° E	7156
Palau	Pacific	07.8045° N	134.9869° E	8021
Philippine	Pacific	10.2213° N	126.6864° E	10,540
Puerto-Rico	Atlantic	19.7734° N	66.9276° W	8526
Ryukyu	Pacific	24.5109° N	127.3602° E	7531
San Cristobal	Pacific	11.2800° S	162.82° E	8641
Santa Cruz	Pacific	12.1800° S	165.7700° E	9174
South Orkney	Southern	60.8510° S	41.0442° W	6820
South Sandwich	Southern	56.2430° S	24.8326° W	8125
Tonga	Pacific	23.2500° S	174.7524° W	10,800[***]
Vitjaz	Pacific	10.2142° S	170.1178° E	6150
Volcano	Pacific	24.3326° N	143.6107° E	8724
Yap	Pacific	08.4073° N	137.9244° E	8292
Trench faults				
Cayman	Atlantic	19.1700° N	79.8633° W	8126
Diamantina	Indian	34.8069° S	102.5667° E	7099
Emperor	Pacific	45.1594° N	174.1444° E	8103
Lira	Pacific	01.3800° N	150.6500° E	6881
Massau	Pacific	01.4200° N	148.7400° E	7208
Romanche	Atlantic	00.2226° S	18.5264° W	7715
Vema	Indian	08.9232° S	67.4983° E	6492
Troughs				
Agulahas	Atlantic	53.8494° S	26.9643° E	6787
Argentina	Atlantic	48.8498° S	50.6501° W	6859
Canaries	Atlantic	24.1248° N	35.6662° W	7268
Central	Pacific	01.1723° S	168.2845° W	8211
Madagascar	Indian	31.3555° S	61.0106° E	7113
North American	Atlantic	26.1278° N	55.8783° W	6922
N.W. Pacific	Pacific	39.8184° N	178.8757° W	8565
Philippine	Pacific	20.8711° N	136.7116° E	7872
S.E. Atlantic	Atlantic	13.3632° S	1.8716° W	6559
South African	Atlantic	45.5201° S	14.4328° E	6509
South Australian	Indian	45.0223° S	128.3304° E	6826
West Australian	Indian	22.2517° S	102.378° E	6600[****]
Zeleniy Mys	Atlantic	14.5810° N	35.2081° W	6708

around 1200 km in length (Angel, 1982); Fig. 1C). The trench is formed by the subduction of the Australian Plate north-east under the Vanuatu archipelago. The New Hebrides and Kermadec trenches are separated by the South Fiji Basin, an abyssal plain that reaches a maximum water depth of ~4100 m. The Basin is bound to the east by the remnant Colville Ridge and its northern extension, the Lau Ridge. To the east the Basin is bound by three elongate topographic highs named, from east to west, Three Kings Ridge, Norfolk Ridge and Lord Howe Rise all broadly oriented north-south. The Norfolk Basin (also known as the New Caledonia Basin) is located between the Norfolk Ridge and Lord Howe Rise. The Mariana Trench is located southeast of the island of Guam and east of the Mariana Islands and is up to 10,984 m deep (Gardner et al., 2014), is 2550 km in length with a mean width of 70 km (Angel, 1982); Fig. 1D). The trench is formed as the Pacific Plate subducts beneath the Mariana Arc System, part of the Philippine Plate, to the west. This study encompasses only the westernmost portion of the Mariana Trench (Fig. 1A), oriented roughly west-east.

2.3. Bathymetry from the study areas

Bathymetry data were derived from the Global Multi-Resolution Topography (GMRT) Synthesis which is a multi-resolution global Digital Elevation Model (DEM) that includes processed multibeam bathymetry data where available (Ryan et al., 2009) and gridded seafloor depths (30 arc-second resolution) derived from GEBCO. These data were sourced from the Marine Geoscience Data System (www.marine-geo.org). ArcGIS grids of the bathymetry data were produced at the best possible resolution of 122 m for the Mariana Trench, 237 m for the Kermadec Trench, and 248 m for the New Hebrides Trench and South Fiji Basin (Fig. 1). Additional layers of slope, bathymetric positioning index and aspect were derived from the bathymetry data and were generated in ArcGIS using the spatial analyst extension and Benthic Terrain Modeler (Wright et al., 2012).

2.4. Seafloor imaging

Images of the seafloor were obtained using two free-fall lander vehicles; the Hadal-lander and the Abyssal-lander (full deployment details are included in supplementary material Table S2).

The Hadal-lander was an 11,000 m rated baited video camera. Its basic delivery system comprised four pairs of 11,000 m rated Vitrovex 17″ buoyancy spheres (Nautilus Marine Services, Germany) that surfaced the lander after jettisoning a 100 kg ballast weight by acoustic command from the surface via a tandem set of acoustic releases (Oceano 2500 ti-Deep, IXSEA, France). The scientific payload comprised a bespoke 3CCD Hitachi colour video camera (800 TV lines), controlled and logged autonomously by a custom built control system (NETmc Marine, UK). Illumination was provided by two LED lamps in 6″ vitrovex spheres. The camera was pre-programmed to take one minute of video every five minutes throughout each deployment and was powered by a 12 V lead acid battery (SeaBattery; DSP&L, USA). The camera records video in a near-horizontal orientation with a 120 cm long tubular arm within view of the camera which included a horizontal scale bar. The field of view was approximately 40° giving ~75 cm scene width at 120 cm in front of the camera. An SBE-39 pressure and temperature sensor (SeaBird electronics, USA) was logging at 30 s intervals throughout at 1 m above the sea floor. The hadal-lander is described in more detail by Jamieson (2015).

The Abyssal-lander was a 6000 m rated baited stills camera that operates in a similar manner to the Hadal-lander. The camera, however, was a 5 megapixel stills camera and flash (Kongsberg Maritime, UK) pre-programmed to take one image every 60 s and was powered by a 24 V lead acid battery (SeaBattery; DSP&L, USA). The camera was situated 2 m above the seafloor looking vertically down with a field of view of 2 × 1.5 m. The lander was equipped with a Seaguard CTD probe (Anderraa, Norway) that recorded every 30 s throughout at 2.5 m above the seafloor. The Abyssal-lander is described in more detail by Linley et al. (2015).

Positional data for all deployments were taken from the vessels Digital Global Positioning System (DGPS) position logged when the free-fall landers were deployed. Water depths were derived using the pressure data acquired from each free-fall lander deployment using the Saunders (1981) method.

2.5. Seafloor classification

The field of view was calibrated using the known dimensions of the bait arm visible in the Hadal-Lander images, of the reference scale in the Abyssal-Lander images and the angles of the cameras as described above. This aided in quantitative analysis of particle-size discrimination of the seabed. A total of 96 images were obtained from the Kermadec,

Mariana and New Hebrides trenches and South Fiji Basin (Fig. 1). The stations spanned water depths ranging from 1554 to 10,980 m with 55 of the stations interrogating water depths > 6000 m. Unfortunately there were no physical samples available where grain-size analysis could be performed by dry sieve or laser diffraction analysis for example. For each digital stills image acquired: (1) a seabed sediment classification was assigned broadly based on Wentworth (1922) and a modified Folk diagram (Folk, 1954; Long, 2006); (2) the potential for recovery of a physical sample of sediment was considered and ranked between 1 and 4 (1 indicates the potential for recovery is high; 2 indicates potential for recovery is moderate; 3 indicates recovery would be unlikely due to gravels, pebbles and cobbles; 4 indicates bedrock cropping out at seabed therefore no recovery of a sediment sample would be possible).

3. Results

3.1. Geographic isolation

Of the 34 subduction trenches and trench faults, 26 are located in the Pacific Ocean (76%), with three of the 13 hadal troughs (23%) also located in the Pacific Ocean. The concentration of hadal areas within the Pacific Ocean, predominantly around the perimeter, is a direct result of the subduction of the Pacific plate below the surrounding tectonic plates. The geographic distance matrix calculated in kilometres, for each point, for all combinations, from a database of deepest points of the 27 subduction trenches (Table 2), 13 troughs and seven trench faults between 6000 m water depth and full ocean depth (the matrix for all 47 hadal zones is included in supplementary material Table S1).

The 47 hadal zones statistically grouped into five significant clusters based on how geographically distant each hadal area is from all other hadal areas (Figs. 2 and 3). Clusters 1 and 3 had the highest approximately unbiased (AU) p-values of ≥95% indicating that they were strongly supported by the data. Cluster 2 had an AU p-value of 89% and cluster 5, the largest cluster, had an AU p-value of 80%. Cluster 4 scored > 99% if the Kurile-Kamchatka Trench was discounted from the cluster, otherwise the AU p-value was 67%.

As expected, the clusters broadly divide into groups by geographic area. Cluster 1 comprise the Agulahas, Argentinian, South African, South Orkney and South Sandwich hadal areas located in the south Atlantic and Southern oceans between 51°W and 27°E, distant from any continental landmass. Cluster 2 comprises the Atacama, Canaries, Cayman, Middle America, North American, Puerto-Rico, Romanche, SE Atlantic and Zeleniy Mys hadal areas located predominantly in the Atlantic Ocean, although the Atacama and Middle America trenches are located in the south-eastern Pacific Ocean in close proximity to the landmasses of South America and Central America respectively. Cluster 3 comprises the Diamantina, Hjort, Madagascar, South Australian, West Australian and Vema hadal areas, located in two areas: the central Indian Ocean, a region with a paucity of hadal areas, and to the west and south of Australia and New Zealand. The hadal areas of cluster 3 are located around 1150 (minimum) to 1800 (maximum) km from significant continental land masses. Cluster 4 is located in the northern Pacific Ocean offshore the Kuril Islands, between Japan and the Kamchatka Penninsula, and south of the Aleutian Islands. The Aleutian, Emperor, Kurile-Kamchatka and NW Pacific trenches make up cluster 4. Cluster 5 encompasses the remaining 23 hadal areas located in the western and south-western Pacific Ocean with the exception of the Java Trench located in the eastern Indian Ocean.

Clusters 4 and 5 are comprised exclusively, with the exception of the Java Trench (Indian Ocean) included within cluster 5, of hadal areas within the Pacific Ocean. Of the remaining hadal trenches and trench faults, three can be found in the Atlantic and Indian oceans (9% respectively), and two are found in the Southern Ocean (6%). In terms of hadal troughs, seven are found in the Atlantic Ocean (54%), and three are located in each of the Indian and Pacific oceans (23% respectively). All hadal areas located in the Atlantic Ocean are members of clusters 1 and 2 with the two trenches located in the Southern Ocean found exclusively in cluster 1. Additionally, the Middle America and Atacama trenches located in the southwestern Pacific Ocean are included in cluster 2. Hadal areas within the Indian Ocean are found exclusively within cluster 3 with the addition of the Hjort Trench (Pacific Ocean) as the fifth member of that cluster.

Cluster 2 comprises members with the highest mean distance from all other hadal zones of 12,325 km (± 4653 S.D.). Cluster 5 has the lowest mean distance of 7637 km (± 5201 S.D.) and is concentrated in a region with the numerical majority of hadal areas in the western Pacific Ocean. Clusters 3 and 4 have means of 8963 km (± 3838 S.D.) and 8848 km (± 4718 S.D.) respectively. Cluster 1 has a mean of 11,128 km (± 4247 S.D.).

3.2. Large-scale topographic variation

Of the 27 hadal trenches, there is no correlation between depth and descriptors of size (area and length). The longest trenches are the Java (~4500 km), Atacama (3700 km) and Aleutian (3700 km) trenches which have depths of 7450, 8074 and 7822 m respectively. In fact, most of the longest trenches are not excessively deep. The five shortest trenches are the Volcano, Yap, Banda, Admiralty and Palau trenches (8724, 8292, 6887 and 8021 m deep respectively) of which the Palau and Admiralty trenches are also among the five smallest trenches in terms of area. The projected area > 6500 m depth gives a far more representative indication of the size of the hadal habitat, irrespective of depth. The largest hadal habitats are found within the Izu-Bonin (99,801 km^{-2}), Kurile-Kamchatka (91,692 km^{-2}), Mariana (79,956 km^{-2}), Tonga (65,817 km^{-2}) and the Aleutian (63,036 km^{-2}) trenches, whereas the smallest are in the Admiralty (4050 km^{-2}), New Hebrides (2439 km^{-2}), Diamantina (2430 km^{-2}), Palau (1692 km^{-2}), and the Middle America (36 km^{-2}) trenches.

There is a linear decrease of habitat area with depth common to all trenches, regardless of whether they are deep (> 10,000 m) or shallower trenches (Fig. 4). In the six deepest trenches, the shallowest 1000 m (6500–7500 m) accounts for an average of 55% ± 7.3 S.D. of the entire trench, whilst the deepest 1000 m accounts for 0.97% ± 0.4 S.D. In six randomly selected mid-depth trenches, the upper 1000 m accounts for an average of 77% ± 7.5 S.D. while the deepest 1000 m is 14% ± 4.1 S.D. of the trench. As an example, in the Kermadec Trench, beyond the relatively flat abyssal plains it decreases linearly ($y = -2336.9x + 16{,}733$; $R^2 = 0.9352$). The area between 6500 and 7000 m spans 17,057.9 km^{-2} (34.3% of the trench) whereas > 10,000 m spans just 15.5 km^{-2}, accounting for just 0.03% of the trench. In fact, the shallowest 50% of the trench in terms of depth (6500–8500 m) accounts for 87.3% of the benthic habitat (43,425 km^{-2}).

Beyond bathymetric issues, the trenches comprise two flanks representing each converging plate; the overriding plate, or fore-arc usually comprising predominantly continental crust, and the underriding oceanic plate. The underriding plate tends to be of a more gradual relief as they constitute what was once the neighbouring abyssal plains gradually travelling down towards the trench axis as it is subducted. The overriding plate tends to be of far steeper relief as it is forced upwards by the underriding plate, thus trenches are asymmetrical. Therefore the trench flank comprising the steeper overriding plate are generally smaller in terms of area. These two flanks are likely to be contrasting with regard to habitat as the fore-arc theoretically hosts many chemosynthetic seeps (Blankenship-Williams and Levin, 2009), as supported by Fujikura et al. (1999) and Fujiwara et al. (2001). Furthermore, the flanks are steeper and likely to comprise rocky outcrops, escarpments and abrupt walls. These types of substrata and seafloor conditions, combined with an increased chemosynthetic-based community may well hosts communities that differ greatly from those at equal depths on the adjacent underriding slopes. The trenches are

Table 2
Geographic distance matrix calculated in kilometres using the semi-major axis of the WGS84 reference system as the default radius of the earth (Ersts [Internet]) for the 27 subduction trenches between 6000 m water depth and full ocean depth (see Table 1). The matrix for all 47 hadal zones is included in supplementary material Table S1.

	Admiralty	Aleutian	Atacama	Banda	Bougainville	Hjort	Izu-Bonin	Kurile-Kamchatka	Japan	Java	Kermadec	Mariana	Middle America	New Britain
Aleutian	6714													
Atacama	14,891	12,848												
Banda	2121	8196	16,025											
Bougainville	830	7109	14,100	2551										
Hjort	6484	12,449	9872	6341	5794									
Izu-Bonin	3455	4311	16,592	4112	4215	9923								
Kurile-Kamchatka	4969	2807	15,621	5834	5639	11,432	1722							
Japan	4136	3831	16,474	4778	4879	10,613	699	1091						
Java	3616	9503	16,047	1515	3933	6205	5246	6935	5845					
Kermadec	4943	9226	10,048	6131	4115	3500	8069	9081	8640	6937				
Mariana	1536	5937	16,222	2260	2361	7895	2051	3714	2750	3650	6452			
Middle America	12,962	8122	4799	15,083	12,627	12,429	12,300	10,930	11,926	16,556	10,266	13,256		
New Britain	720	7375	14,483	2027	531	5770	4158	5689	4845	3404	4444	2180	13,156	
New Hebrides	3513	8353	11,443	4840	2688	4102	6679	7803	7275	5830	1432	5020	11,059	3041
Palau	1849	6723	16,735	1536	2637	7651	2576	4298	3245	2795	6723	908	14,164	2280
Philippine Trench	2785	7045	17,627	1800	3547	8140	2738	4394	3304	2549	7579	1726	14,853	3145
Puerto-Rico	15,541	9421	4826	17,527	15,383	14,439	13,673	11,988	13,079	18,919	13,047	15,307	2899	15,892
Ryukyu	3665	5786	18,131	3350	4495	9651	1622	3004	1957	4088	8605	2160	13,876	4233
San Cristobal	1906	7291	12,992	3572	1114	5268	5060	6293	5678	4838	3072	3384	11,780	1574
Santa Cruz	2225	7303	12,668	3904	1447	5194	5291	6458	5892	5152	2798	3679	11,485	1910
South Orkney	13,143	16,947	4777	12,631	12,429	6659	16,571	18,027	17,267	11,818	8974	14,523	9519	12,429
South Sandwich	13,693	17,900	5243	12,828	13,055	7269	16,934	18,637	17,606	11,802	9882	14,923	10,041	12,973
Tonga	4625	8253	10,267	6147	3837	4486	7459	8303	7975	7171	998	6051	9762	4259
Vitjaz	2535	6984	12,376	4354	1830	5471	5340	6370	5899	5644	2742	3895	10,974	2333
Volcano	2840	4700	16,486	3583	3608	9306	617	2277	1310	4805	7516	1447	12,516	3542
Yap	1616	6485	16,501	1721	2429	7651	2432	4144	3119	3065	6540	594	13,840	2123

	New Hebrides	Palau	Philippine Trench	Puerto-Rico	Ryukyu	San Cristobal	Santa Cruz	South Orkney	South Sandwich	Tonga	Vitjaz	Volcano
Aleutian												
Atacama												
Banda												
Bougainville												
Hjort												
Izu-Bonin												
Kurile-Kamchatka												
Japan												
Java												
Kermadec												
Mariana												
Middle America												
New Britain												
New Hebrides												
Palau	5309											
Philippine Trench	6185	951										
Puerto-Rico	13,945	16,140	16,380									
Ryukyu	7173	2029	1592	14,870								
San Cristobal	1644	3744	4660	14,637	5542							
Santa Cruz	1388	4069	4990	14,356	5839	337						
South Orkney	10,227	14,123	14,312	9271	15,896	11,736	11,569					
South Sandwich	11,064	14,363	14,351	9337	15,850	12,487	12,357	1068				

(*continued on next page*)

Table 2 (*continued*)

	New Hebrides	Palau	Philippine Trench	Puerto-Rico	Ryukyu	San Cristobal	Santa Cruz	South Orkney	South Sandwich	Tonga	Vitjaz	Volcano
Tonga	1340	6468	7383	12,631	8204	2725	2401	9792	10,745			
Vitjaz	1448	4380	5320	13,839	6042	807	523	11,665	12,511	2166		
Volcano	6112	2056	2383	14,116	1646	4481	4725	15,957	16,363	6948	4805	
Yap	5116	331	1251	15,883	2115	3522	3840	14,199	14,503	6240	4126	1873

also exposed to frequent, seismically induced landslides and turbidity currents. These catastrophic events, reshape vast areas of seafloor in relatively short periods of time (Itou et al., 2000; Fujiwara et al., 2011; Oguri et al., 2013) irrespective of depth, but are again more likely to occur on the overriding flanks than the underriding, further suggesting potentially contrasting environments and stability within a trench irrespective of depth.

The flanks are of course also subjected to the decrease in area with depth, but the asymmetry of the trenches in cross section results in two flanks of differing size. Again, using the Kermadec Trench as an example, the total area of the trench can be divided into an eastern (underriding) slope which covers an area of 32,998 km^{-2} and an western (overriding) slope of only 15,832 km^{-2}. These areas account for 66.5 and 33.5% respectively of the trench > 6500 m, meaning that the underriding slope is nearly twice as large as the overriding slope in terms of benthic habitat. The mean slope on the overidding west side is 7.7° ± 1.2 S.D. and on the underridding east side is 5.9° ± 1.8 S.D. As the overidding plates are generally always steeper than the underridding plates, the asymmetry means that the underidding plate will always be larger.

3.3. Seafloor heterogeneity

The bathymetry data show that the most conspicuous features of the Kermadec and Mariana trenches are an extensive network of elongate ridges and troughs interpreted as the seafloor expression of normal fault scarps on the underriding plate (Pacific Plate) seaward of the trench axis (Fig. 1B and D). These faults can be detected 55 km seaward from the axis of the Kermadec Trench (Fig. 5) coincident with the onset of the 5500 m bathymetric contour in the north-northeast and 6500 m bathymetric contour in the south-southwest, and as far as 100 km from the axis of the Mariana Trench (Fig. 6A) coincident with the 4500 m bathymetric contour. Within the Kermadec Trench the fault scarps are most prolific between approximately 34°20′N and the intersection with the Louisville seamount chain at approximately 25°40′S, where they continue to form a prominent seafloor feature over the entire length of the Tonga Trench. The faults may still exist cropping out at seabed at locations even further from the trench axis but they are not resolved in the resolution of data available to this study.

The strike of the faults within the Mariana Trench are roughly parallel to the trench axis in the westernmost part of the study area (Fig. 6A) but become oblique to the axis further east (Fig. 6B). The seafloor offsets are up to 1000 m in the vicinity of the trench axis, but reduces to 120–200 m offset as the distance away from the axis increases seaward. Within the Kermadec Trench the fault strikes are roughly parallel to sub-parallel to the trench axis (Fig. 5B and C) with seafloor offsets frequently between 400 and 1200 m (Fig. 6C) within 30 km of the trench axis, reducing to 150–400 m offset with increasing distance from the trench axis. Slope angles associated with the fault scarps are typically between 10° and 40° with slopes frequently in excess of 25°. The escarpments are laterally continuous with the throw, or vertical offset, decreasing towards the escarpment ends.

In addition, the normal faults form horst and graben structures which create seafloor depressions where sediment can pond (e.g. Figs. 6C, 7A and E within the Kermadec Trench; Fig. 7B within the Mariana Trench), and cut other large scale topographic features such as seamounts (Figs. 5B and 7E). Sedimentary ponds, or small sedimentary basins, are typically areas of relatively flat topography where slope angles are predominantly < 4° (e.g. Fig. 7A and B) and can be up to 45 km in length. Pinnacles and larger seamounts are observed on the available bathymetry data throughout the three study areas (Fig. 1B–D). Within the Kermadec Trench pinnacles are also observed within a number these sedimentary basins, or ponds, forming conical features up to 750 m in height (Fig. 6C) although smaller examples, up to 100 m in height, are also present (see Fig. 7A coincident with photograph A1). Areas of 'rough' seafloor texture are also evident (e.g.

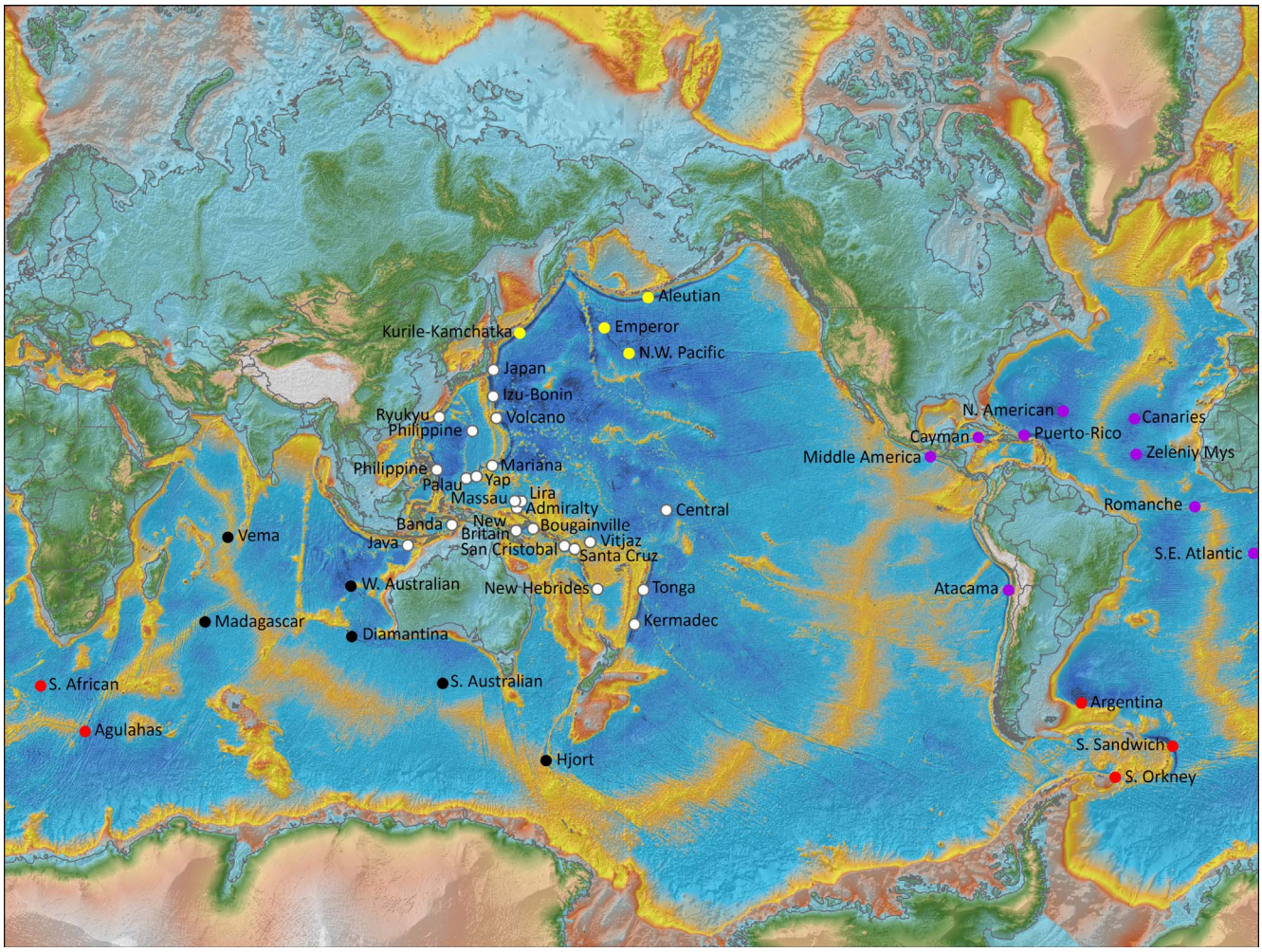

Fig. 2. Map illustrating the geographic distribution of the five 'isolation' clusters of the 47 hadal areas between 6000 m and full ocean depth. The colours represent: cluster 1 (red), cluster 2 (purple), cluster 3 (black), cluster 4 (yellow), cluster 5 (white). All elevation data sourced from the Global Multi-Resolution Topography (GMRT) Synthesis (Ryan et al. 2009). (For interpretation of the references to colour in this figure legend, the reader is referred to the web version of this article.)

Fig. 6B) on the underriding plate although it is currently unclear what may be the cause of this.

A series of clearly defined seafloor ridges are also observed on the overriding plate in both the Mariana and Kermadec trenches, although are best imaged within the Kermadec Trench (Fig. 7A and B) and in the south-southwest–north-northeast oriented Hikurangi Trough (Figs. 7C and 8D). These elongated features are the seafloor expression of thrust faults within the imbricate thrust zone of the accretionary wedge. These ridges form slopes generally up to 15°, although locally can exceed 20°. Mass wasting scars and slump features are also evident in the topography of the overriding plate and are particularly evident in the southern Kermadec Trench (Fig. 7C) forming amphitheatre shaped head walls.

Although no significant topographic features such as thrust faults, normal faults and a defined accretionary wedge were identified within the New Hebrides Trench in this study, this is likely due to a lack of high-resolution data (e.g. bathymetry data) rather than conclusive evidence of their absence at this location.

Photographic ground-truthing from the Kermadec, Mariana and New Hebrides trenches and South Fiji Basin confirm that there is not only significant topographic variation but also significant variation in the distribution of seafloor sediments (Figs. 7 and 8) within these deep-sea areas.

Overall, eight categories of seabed substrate were identified: bedrock, bedrock and fine-grained mud, bedrock and gravelly mud, cobbles and pebbles, muddy gravel, gravelly fine-grained sediment, slightly gravelly fine-grained sediment, and fine grained-sediment. A summary of the results from the analysis is presented in Table 3 (all images analysed are included in supplementary material Figs. S2–S4).

Stations from the Kermadec Trench comprised all but one of the identified seabed sediment categories (bedrock and gravelly mud) from stations covering water depths from 1000 to 9281 m. Within the Hikurangi Trough, 22 stations sampled water depths from 1554 to 6191 m water with the most commonly observed sediment class being fine-grained sediment (n = 12), followed by gravelly fine-grained sediment (n = 4), and bedrock cropping out at seabed (n = 3). Muddy gravel (n = 1), cobbles and pebbles (n = 1), and slightly gravelly fine-grained sediment (n = 1) were only observed rarely. Two further stations in water depths of 1000 and 1481 m were acquired close to New Zealand on the Hikurangi Plateau and comprised fine-grained sediment. Within the Kermadec Trench proper, 11 stations sampled water depths between 1974 and 5646 m, and were dominated by fine-grained sediment (n = 6), with fewer occurrences of slightly gravelly fine-grained sediment (n = 2), bedrock (n = 1), bedrock and fine-grained sediment (n = 1) and muddy gravel (n = 1). Twelve stations were acquired between 6037 and 7905 m water depth where equal observations of gravelly fine-grained sediment and fine-grained sediment (n = 3 respectively), with slightly gravelly fine-grained sediment, bedrock, and muddy gravel (n = 2 respectively) were recorded. The four stations acquired between 8215 and 9281 m water depth reveal fine-grained

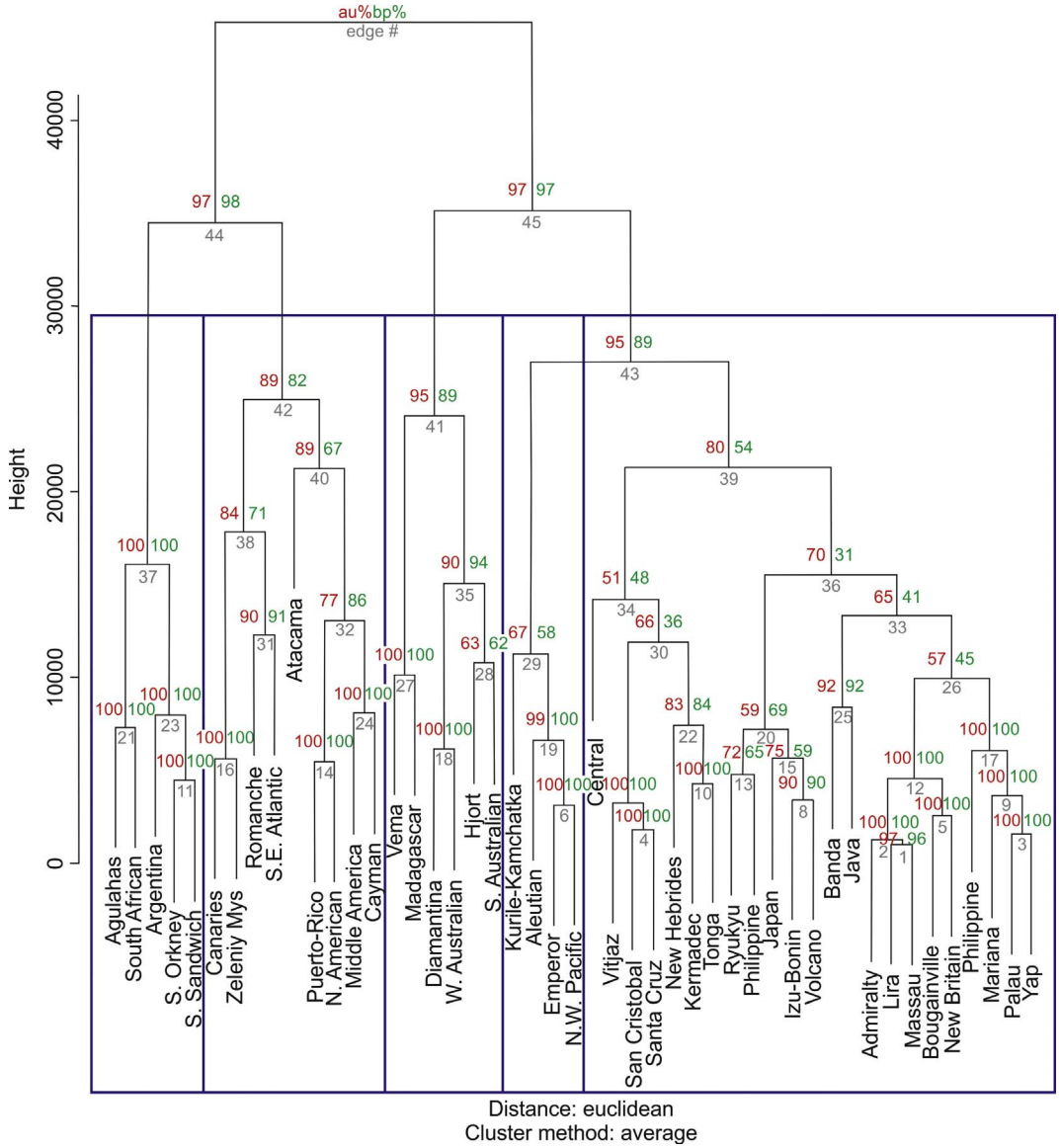

Fig. 3. Dendrogram of hierarchical cluster analysis of distance data measuring the relative 'isolation' of each hadal area from every other hadal area. The five isolation clusters identified by the analysis are delineated by the blue boxes. Red numbers represent the approximately unbiased (au) p-value and green numbers indicating the bootstrap probability (bp) value. (For interpretation of the references to colour in this figure legend, the reader is referred to the web version of this article.)

sediments (n = 3) and slightly gravelly fine-grained sediment (n = 1).

In the Mariana Trench all but one of the seabed sediment categories (cobbles and pebbles) were observed from 31 stations from water depths ranging from 4506 to 10,890 m. Six stations were acquired in water depths from 4506 to 5641 m with the dominant seabed sediment observed comprising muddy gravel (n = 3), with one observation each of bedrock, bedrock and fine-grained sediment and gravelly fine-grained sediment. Fifteen stations sampled water depths from 6008 to 7941 m with gravelly fine-grained sediment dominating (n = 6). Fine-grained sediment (n = 4), bedrock (n = 3), slightly gravelly fine-grained sediment (n = 1) and muddy gravel (n = 1) were also observed within this depth range. Between 8000 and 10,890 m water depth, 10 stations observed fine-grained sediment (n = 3), slightly gravelly fine-grained sediment (n = 2), gravelly fine-grained sediment (n = 2), bedrock (n = 2), and bedrock and gravelly mud (n = 1).

Six stations were sampled from the New Hebrides Trench in water depths from 2086 to 5344 m, with four stations sampling water depths from 6082 to 6896 m. Gravelly fine-grained sediment was observed as the dominant seabed sediment classification in the shallower stations (n = 3), followed by slightly gravelly fine-grained sediment (n = 2) and fine-grained sediment (n = 1). From the deeper stations fine-grained sediment was observed most frequently (n = 2), with equal representation of bedrock and slightly gravelly fine-grained sediment (n = 1 each).

The three stations from the South Fiji Basin interrogated 4078–4100 m water depth and comprised slightly gravelly fine-grained sediment (n = 2) and gravelly fine-grained sediment (n = 1).

Overall, the 95 stations suggest that the Mariana Trench comprises more gravel-rich sediments than both the Kermadec and New Hebrides trenches and the South Fiji Basin, furthermore more bedrock is seen cropping out at seabed within the Mariana Trench. Whereas data from the Kermadec Trench suggest fine-grained sediment dominates. However the relationship is more complicated as the analysis confirm that there is no correlation between the eight seabed substrate classifications and water depth (Fig. 9), geological setting (overriding plate, underriding plate or trench axis) or indeed between the Kermadec, Mariana and New Hebrides trenches and South Fiji Basin (Table 3). All eight substrate classifications defined in this study were represented at the 40 stations acquired in water depths < 6000 m, with five represented at the 41 stations acquired in water depths 6000–8000 m,

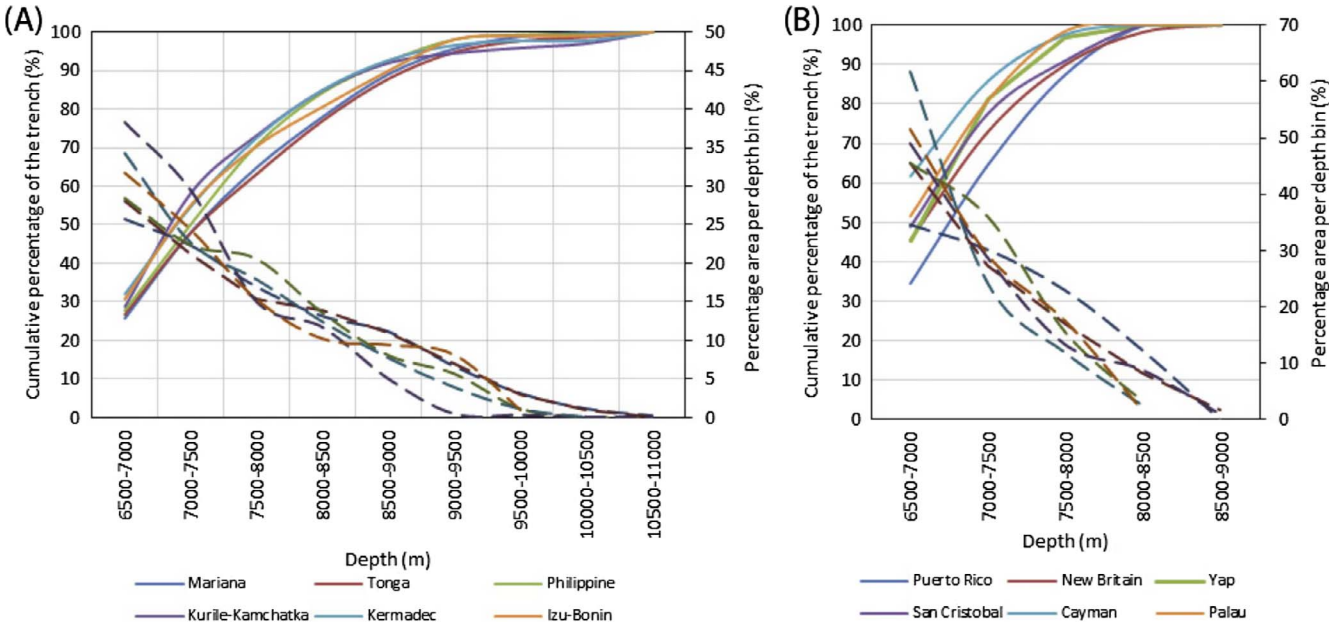

Fig. 4. Decrease in habitat size with increasing water depth (dashed lines) and cumulative area of trench with depth (solid lines) illustrated in percentage of trench per 500 m depth bin for the six deepest trenches (A) and six randomly selected shallower trenches (B) ().
adapted from Jamieson 2015

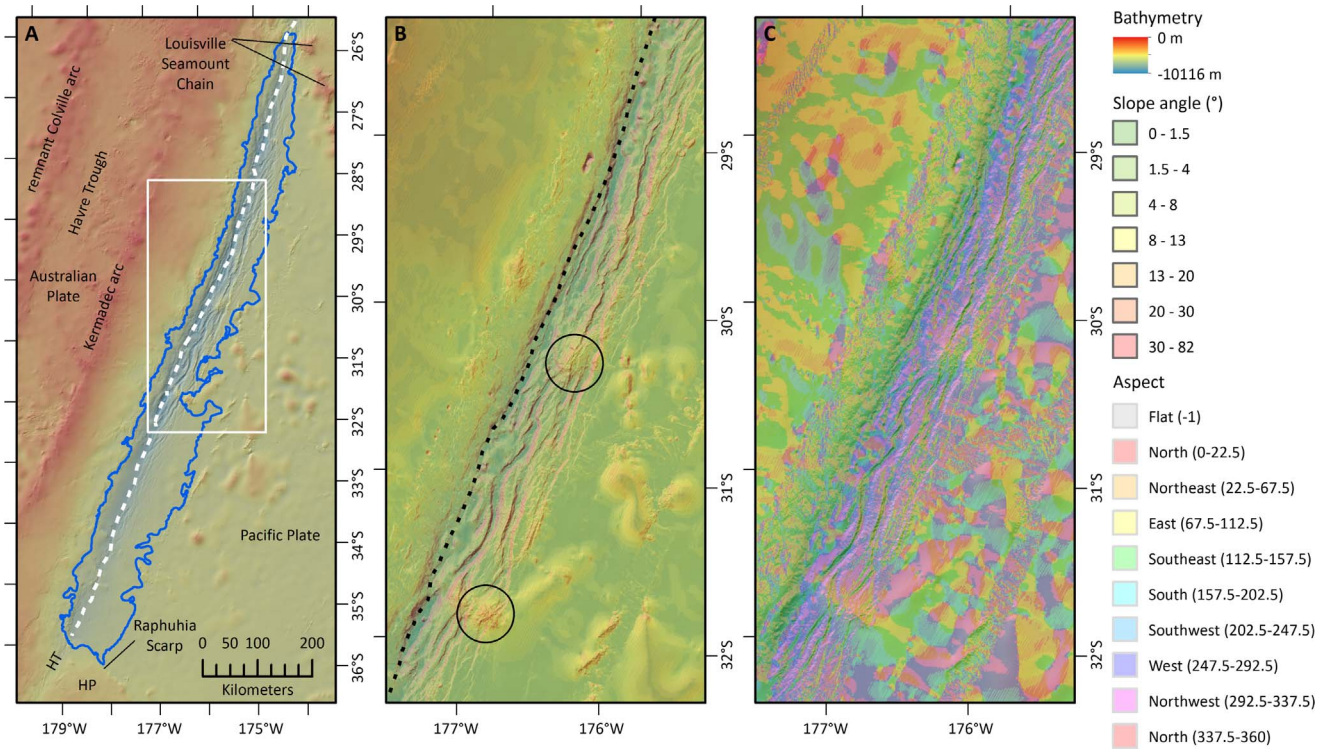

Fig. 5. (A) Overview of the Kermadec Trench showing major structural features. The dashed white line is the trench axis. The blue line is the 6000 m contour. The white box is the location of maps (B) and (C). HP = Hikurangi Plateau; HT = Hikurangi Trough. For location see Fig. 1A. (B) Slope map overlain on the bathymetry, highlighting normal fault scarps (red/orange regions) prevalent on the Pacific Plate. The black dashed line is the trace of the deformation front. Seamounts cut by normal faulting are encircled in black. (C) Aspect map overlain on the bathymetry, highlighting the trench axis and strike of the normal faulting prevalent on the Pacific Plate. (For interpretation of the references to colour in this figure legend, the reader is referred to the web version of this article.)

and five represented at the 14 stations acquired in water depths 8000 m to full ocean depth.

There are however, a number of interesting and sometimes surprising examples of seafloor heterogeneity observed in the seafloor images and it is clear that there is no firm guideline as to predicting the distribution of seabed sediments and bedrock occurrence based on the data available (e.g. Fig. 9). Photographs A1 (see also Fig. 8F) and A2 (Fig. 7A) from the Hikurangi Trough are located < 200 m apart, yet show fine-grained sediment representing the seafloor sediments of the basin, and a view over the edge of the steep sloped pinnacle around 100 m in height. Perhaps most interesting are images showing indications of mass wasting events on the overriding plate from the Kermadec

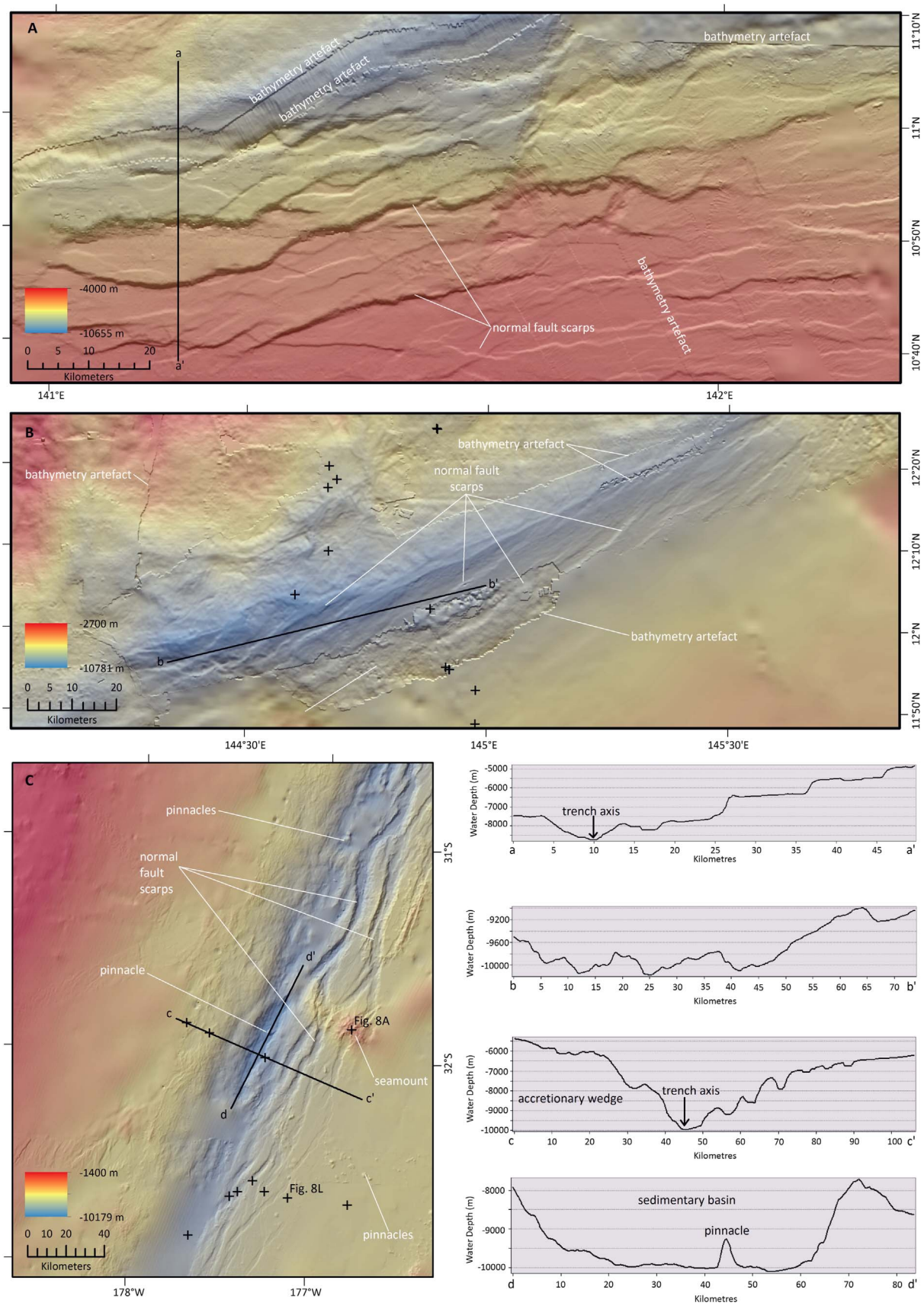

Fig. 6. Maps showing (A) oblique lineaments present in the seafloor of the western Mariana Trench (for location see Fig. 1D) and corresponding cross section illustrating relative variation in local topography that can exceed 1000 m; (B) oblique lineaments and rough seafloor topography of the Mariana Trench, south of Guam (for location see Fig. 1D). The corresponding cross section illustrates the topographic variation between ridges and troughs to exceed 400 m; (C) oblique lineaments, pinnacle and a seamount in the seafloor of the Kermadec Trench (for location see Fig. 1B). Corresponding cross-sections show steeper overriding plate (western trench flank) compared with the more gently sloping underriding plate (eastern trench flank) in addition to oblique lineaments forming ridges and troughs > 500 m high, and a pinnacle (~750 m high) located within the trench axis in what appears to be a sediment infilled basin. Note not all features are labelled, only a representative selection. Abyssal-lander and Hadal-lander deployments are indicated by black crosses.

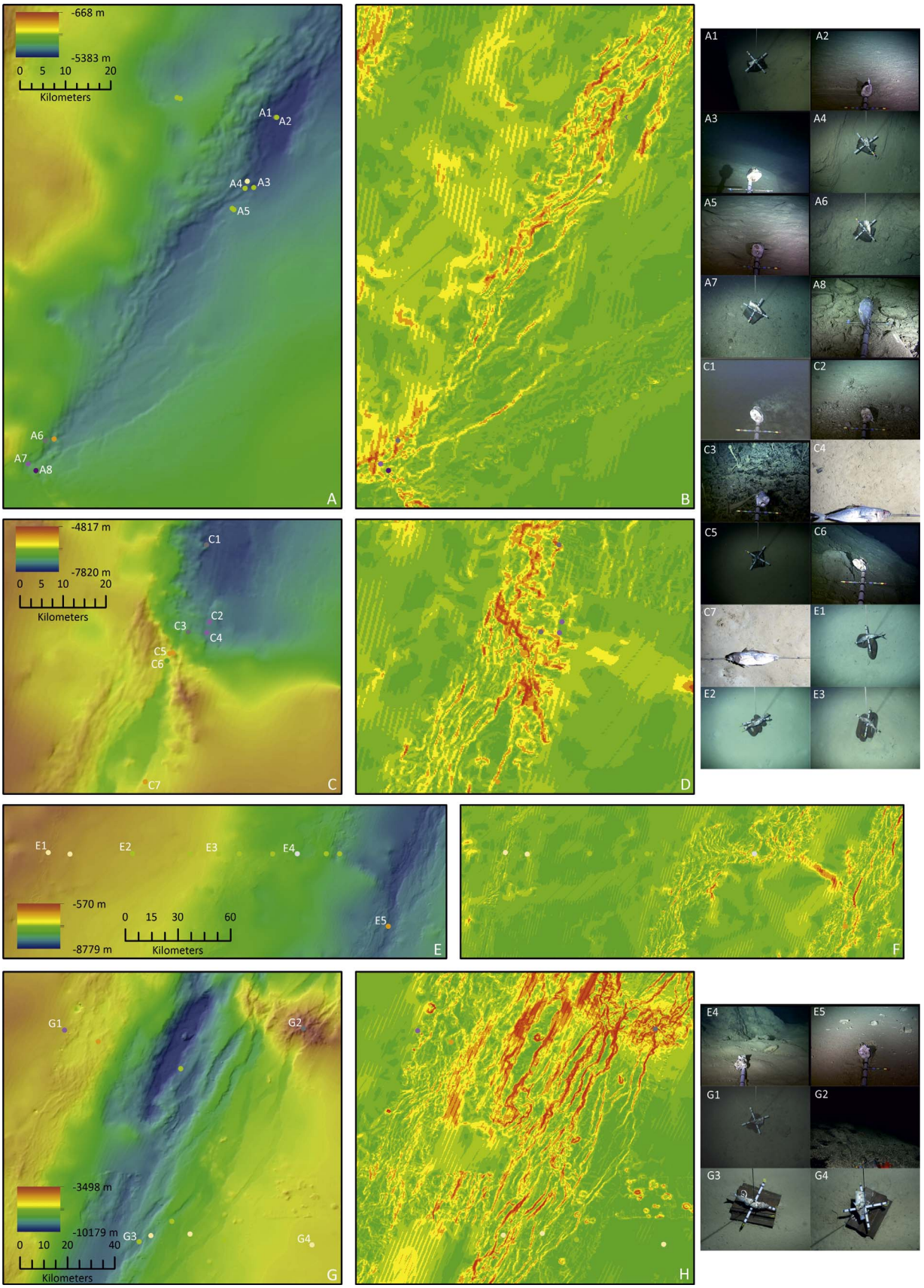

Fig. 7. (A) Area of the Hikurangi Trough, southwest of the Kermadec Trench. Selected seafloor photographs are indicated with corresponding seabed sediment classification; (B) corresponding slope map for (A); (C) area where the Hikurangi Trough enters the Kermadec Trench. Selected seafloor photographs are indicated with corresponding seabed sediment classification; (D) corresponding slope map for (C); (E) area of the Kermadec Trench showing a sedimentary pond with a pinnacle approximately 750 m in height and normal faults cropping out on the seafloor (see also Fig. 6C). Selected seafloor photographs are indicated with corresponding seabed sediment classification; (F) corresponding slope map for (E); (G) area of the overriding Australian Plate showing the deformation front and trench axis. Selected seafloor photographs are indicated with corresponding seabed sediment classification; (H) corresponding slope map for (G); (I) map of the Kermadec Trench showing location of inset maps. The blue line is the 6000 m contour.

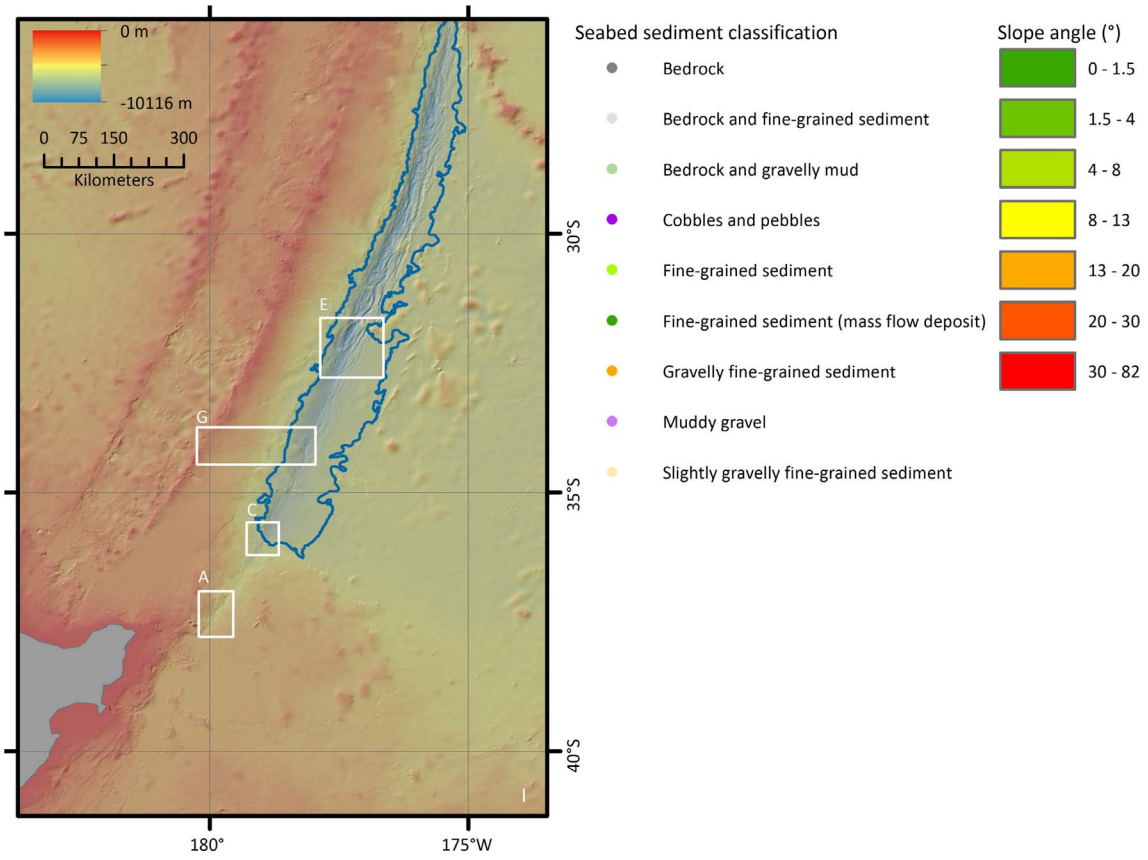

Fig. 7. (*continued*)

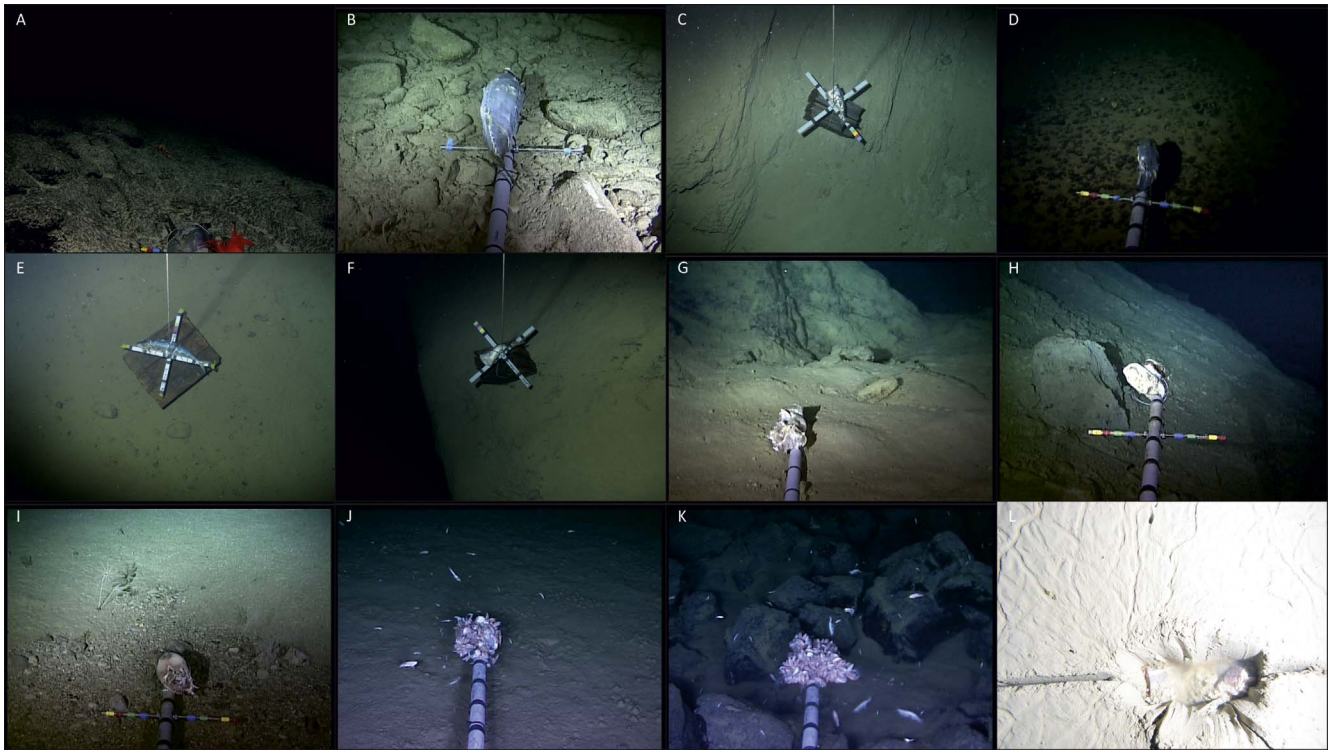

Fig. 8. Selected seafloor images from the Kermadec (Kerm), Mariana (Mar) and New Hebrides (NHeb) trenches; (A) pillow basalts cropping out at sea bed on the summit of a seamount (Kerm, 3655 m), (B) cobbles and pebbles with a fine-grained sediment veneer (Kerm, 3975 m), (C) bedrock with bedding evident and a fine-grained sediment veneer (Kerm, 4953 m), (D) muddy gravel (Mar 5044 m), (E) gravelly fine-grained sediment (NHeb, 5215 m), (F) bedrock with fine-grained sediment veneer, escarpment edge is clearly visible (Kerm, 5295 m), (G) fine-grained sediment with bedrock outcrop protruding above level of surrounding seafloor (Kerm, 5601 m), (H) mass flow deposit comprised of fine-grained sediment (Kerm, 6191 m), (I) muddy gravel with the boundary between substrate types clearly visible (Kerm, 7243 m), (J) fine-grained sediment (Mar 8000 m), (K) blocky/fractured bedrock outcrop (Mar 8098 m), (L) fine-grained sediment with lebensspuren (Kerm, 9281 m). For location see Figs. 1 and 6. For all 95 images analysed see supplementary material Figs. S2–S4.

Table 3
Summary of the image analysis within the Kermadec, Mariana and New Hebrides trenches and the South Fiji Basin. AP = abyssal plain, OP = overriding plate, SM = seamount, TA = trench axis, UP = underriding plate. All images analysed are included in supplementary material Figs. S2–S4.

Sea-bed sediment classification	Number of sea-bed photographs										
	Kermadec Trench				Mariana Trench			New Hebrides Trench and South Fiji Basin			
	SM	OP	UP	TA	OP	UP	TA	AP	OP	UP	TA
Fine-grained sediment		13	4	9	3	2	2		1		2
Muddy gravel		1		3	3	1					
Bedrock	1			5	5	1			1		
Slightly gravelly fine-grained sediment		2	3	1	1	1	1	2	2		1
Gravelly fine-grained sediment		1		6	2	6	1	1	3		
Cobbles and pebbles				1							
Bedrock and fine-grained sediment		1				1					
Bedrock and gravelly mud					1						
Sub-total	1	18	7	25	15	12	4	3	7	0	3
Total	51				31			13			

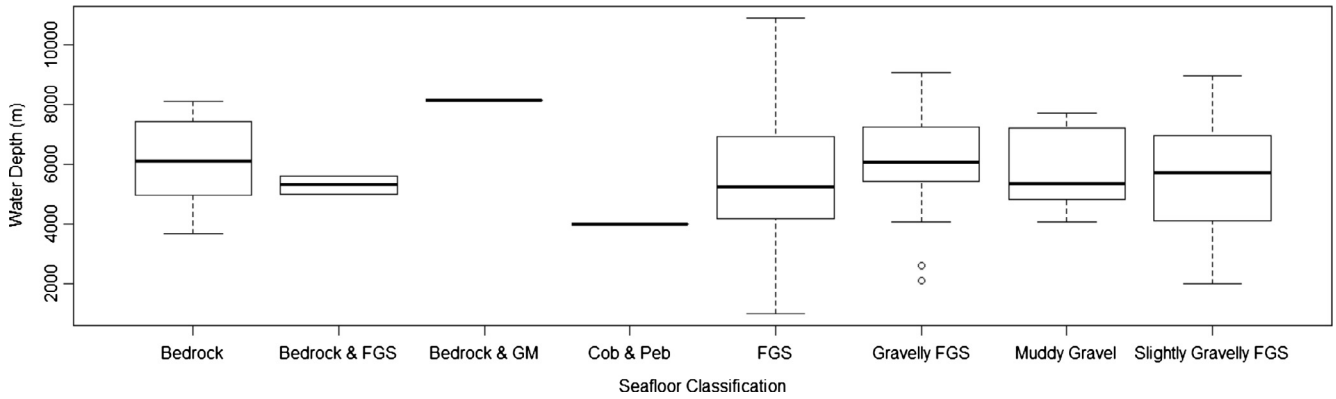

Fig. 9. Boxplot illustrating the distribution of seafloor classifications with water depth within the Mariana, Kermadec and New Hebrides trenches and the South Fiji Basin. FGS = fine-grained sediment, Cob & Peb = Cobbles and Pebbles, GM = Gravelly Mud.

Trench (A3 and C6 on Fig. 7) including a probable block fall (Fig. C6 on Figs. 7 and 8H) where the fresh edges indicate the fall was relatively recent.

Stations forming transects down the accretionary wedge of the overriding plate from both the Kermadec and Mariana trenches show bedded sediments (e.g. Fig. 8C) and basement rocks (e.g. Fig. 8 K) likely basaltic in composition, cropping out at seabed in conjunction with observations of gravel rich (e.g. Fig. 8D and E) and fine-grained sediments (e.g. G2 and G3 from Fig. 7G). Of particular interest is the observation of metre-scale variability in seafloor composition (e.g. Fig. 8E) which may be representative of mass wasting events or oceanographic currents.

4. Discussion

4.1. Sedimentation, food supply and biochemical province

Trenches are considered to be regions where the sedimentation rates are considerably high (Belyeav, 1989). Depending on the nature of the relief and geographic location the rates and composition of sedimentation will vary between trenches and within different sections of the trench flanks and axis. The supply rate and the size of particles decreases with distance from land (Thistle 2003), therefore within trenches adjacent to large continental land masses, sedimentary deposits are dominated by coarser grained sand and silt of terrestrial origin.

The complex internal topography within the trenches results in highly variable sedimentary depositional morphology, such as trench fans, axial channels, ponded sediments within basins and axial sediment lobes (e.g. the Peru-Chile Trench; Thornburg and Kulm, 1987). Nozaki and Ohta (1993) found that the lower sediments from 9750 m in the Izu-Bonin Trench were terrestrial derived and the upper layers were of contemporary marine origin. They also found that the sedimentation rate was of an order magnitude greater than at 8800 m in the neighbouring Japan Trench as a result of turbidity currents via proximity to islands and the nearby Asian continent.

In addition to the 'routine' input of material, sedimentary perturbations occur by episodic lateral transport of particulate material from coastal regions to the deep sea, initiated by earthquakes (Heezen and Ewing, 1952; Garfield et al., 1994; Thunell et al., 1999). This process is also observed directly and indirectly in trenches (Itou et al., 2000; Fujioka et al., 1993 respectively). It is widely accepted that, unlike subaerial landslides, submarine landslides can occur on slopes with gradients as low as 0.5° (e.g. Gage and Tyler, 1991; Masson et al., 2006; Randolph and Gourvenec, 2011) resulting in the relocation of large volumes of sediment, hundreds of metres thick and thousands of metres long. The gradients of the trench flanks are much greater than this, thus it is likely the magnitude of seismically induced sediment perturbation is exacerbated in trenches (Itou et al., 2000; Oguri et al., 2013). Rock fragments are frequently deposited on the trench floors, having fallen from the upper slopes during sediment and rock slides caused by the high seismic activity in the trenches. This study confirms that block falls occur within trench environments and these are comparable to those documented within submarine canyons (Carter et al. 2018).

In addition, the persistent rain of particulate organic matter (POM) from the surface layers and turbidites are deposited along the trench

Table 4
The biogeochemical provinces of each of the major subduction trenches (> 6500 m water depth) with the annual primary production rate in the overlying surface waters. Data taken from Longhurst (2007). *Indicates an average rate between PSAG East and West. The mean POC flux per unit area and the total POC flux per trench are derived from the Lutz et al. (2007) model by M.C. Ichino (NOCS, UK). ¥Indicates values taken from New Britain Trench to derive Total Trench POC flux as no data exists presently. ¤Indicates an average rate between Izu-Bonin and Mariana trenches taken to derived Total Trench POC flux as no data exists presently.

Trench	Biogeochemical province	Province primary production rate ($g\,C\,m^{-2}\,yr^{-1}$)	Mean POC flux ($g\,C\,m^{-2}\,yr^{-1}$ ± S.D.)	Total trench POC flux ($g\,C\,yr^{-1}$)
Banda	Sunda-Arafura Seas Coastal (SUND)	328	1.60 ± 0.44	160.46
Java	Sunda-Arafura Seas Coastal (SUND)	328	1.06 ± 0.62	252.45
Atacama	Chile-Peru Current Coastal (CHIL)	269	3.17 ± 1.43	997.24
Kurile-Kamchatka	Pacific Subarctic Gyre (PSAG)	264	2.26 ± 0.77	3118.86
Aleutian	Pacific Subarctic Gyre (PSAG)	232*	1.76 ± 0.87	1827.27
Philippine	Kuroshio Current (KURO)	193	0.69 ± 0.21	395.12
Ryukyu	Kuroshio Current (KURO)	193	0.90 ± 0.54	145.05
Japan	Kuroshio Current (KURO)	193	3.05 ± 0.91	909.87
South Sandwich	Antarctic (ANTA)	165	0.66 ± 0.28	384.57
Izu-Bonin	North Pacific Subtropical Gyre (NPST)	110	1.69 ± 0.54	1595.41
Puerto-Rico	North Atlantic Tropical Gyre (NATR)	106	0.85 ± 0.33	505.09
New Britain	Western Pacific Archipelagic Deep Basins (ARCH)	100	1.07 ± 0.55	110.29
San Cristobal	Western Pacific Archipelagic Deep Basins (ARCH)	100	0.82 ± 0.47	37.15
New Hebrides	Western Pacific Archipelagic Deep Basins (ARCH)	100	0.86 ± 0.75	18.15
Bougainville	Western Pacific Archipelagic Deep Basins (ARCH)	100¥	1.07¥	79.43
Tonga	South Pacific Subtropical Gyre (SPSG)	87	0.99 ± 0.30	711.16
Kermadec	South Pacific Subtropical Gyre (SPSG)	87	1.64 ± 0.45	1270.33
Volcano	North Pacific Tropical Gyre (NPTG)	85¤	1.12¤	254.22¤
Yap	Western Pacific Warm Pool (WARM)	82	0.56 ± 0.29	67.99
Palau	Western Pacific Warm Pool (WARM)	82	0.61 ± 0.36	11.51
Mariana	North Pacific Tropical Gyre (NPTG)	59	0.55 ± 0.20	606.59

axis (von Huene and Scholl, 1991; Turnewitsch et al., 2014). This input has an incredibly strong spatial and temporal influence on species composition and abundance (Gage, 2003) as the deep sea is essentially a heterotrophic environment where most of the available food is surface derived (Tyler, 1995). POM flux is therefore largely driven by the overlying biogeochemical province. Longhurst (2007) estimated the annual primary production in 57 distinct biogeochemical ocean provinces, based on monthly mean near-surface chlorophyll fields for 1979–1986. The provinces were specified from regional oceanography and through examining the chlorophyll fields. The net primary production rate ($g\,C\,m^{-2}\,yr^{-1}$) can be used as a proxy for relative food supply in each of the trenches, in their respective biogeochemical provinces. These values are given in Table 4. The trenches that underlie the most productive province, the Sunda-Arafura Sea Coastal (SUND), are the Banda and Java trenches. The most oligotrophic provinces overlie the Mariana and Volcano trenches in the North Pacific Tropical Gyre (NPTG). By comparison, the annual primary production overlying the trenches of the SUND province is ~5.5 times higher than those underlying the NPTG province. This is, of course, a rather rough estimate of the relative food supply to each trench. The use of particulate organic carbon (POC) flux models (Lutz et al., 2007) provides a more accurate representation of both POC flux and total POC input, accounting for the size of the trench.

Estimated mean POC flux value predicts that trenches such as the Japan, Kurile-Kamchatka and Atacama trenches receive a relatively high amount of POM compared to the other trenches (reported in Jamieson (2015) based on Lutz et al. (2007) model). Trenches underlying regions of low productivity are predictably oligotrophic, as inferred from the biogeochemical province values (Table 4). However, the indication that some of the trenches are likely to receive the highest POC input based on the biogeochemical province (e.g. Banda and Java trenches) is not supported by the Lutz et al. (2007) model.

The delivery of POM to the trenches differ compared to on the surrounding abyssal plains in the way that it is distributed on the seafloor. The distribution of settled particles is thought to be affected by the physical topography of the trenches. The steep slopes create a gravity- driven downward transport and therefore a subsequent accumulation of POM along the trench axis (Otosaka and Noriki, 2000; Danovaro et al., 2003, Romankevich et al., 2009). This is further driven by occasional seismic induced mass transport of sediments towards the axis (Itou et al., 2000; Rathburn et al., 2009); an effect that is not possible on the flat abyssal plains. This increased availability of food along the trench axis, or the 'trench resource accumulation depth' (TRAD; *sensu* Jamieson et al., 2010) results in the quantity of food on the trench axis and slopes being respectively higher and lower than what would have otherwise fallen on the flat plains.

4.2. Large-scale topographic and bathymetric variation

Trench interior topography, to some degree shares similarities with other features such as submarine canyons where sediment accumulation occurs (Vetter and Dayton, 1998; Tyler et al., 2009; De Leo et al., 2010). Trenches, however, do not exhibit an open end where material can be flushed out into the wider neighbouring abyssal plains (Canals et al., 2006; Arzola et al., 2008), although large depth gradients and steep slopes are likely similar. Trenches also differ from other sloped environments such as continental slopes and rises in that the area of seafloor diminishes with depth, culminating at a single point (the deepest point), rather than a steady continuation of the slope with depth.

Furthermore, evidence presented here illustrates the two contrasting slope model is complicated further with the influence of food supply; primarily surface derived organic particulates that rain into the trench regardless of depth, slope or habitat. The characteristic asymmetrical V-shape cross section of a trench is thought to result in an accumulation of sediment/particulates at the trench axis that may not have otherwise occurred on the flatter abyssal plains (Nozaki and Ohta, 1993; Danovaro et al., 2003; Glud et al., 2013). Trenches are topographically enclosed and therefore deposited material is contained while slowing migrating downwards, driven by gravity, aided by seismic activity, towards the deepest point in the trench axis without any possibility of dispersal (Oguri et al., 2013).

The accumulation of this organic matter (food resource) at the axis, and potentially higher sedimentation from the upper areas, when compared to equivalent depths on already contrasting adjacent slopes, must likely result in habitat alteration regardless of depth and therefore heterogeneity in benthic community compositions. The magnitude, significance and consequences of this ultimately depend on combinations of the biogeographic province (Longhurst, 2007), proximity to land mass and seismic volatility. Therefore irrespective of depth, the larger trench interior, in terms of habitat, could be reasonably categorised into overriding slope, underriding slope and trench axis.

There is a culture of coining 'deeps'; confined areas that represent the deepest part of a trench (and therefore a sub-zone of the trench axis) that may or may not actually represent a distinct morphological feature. For example, the 'Ramapo Deep' in the Izu-Bonin Trench (Fisher, 1954), the 'Horizon Deep' in the Tonga Trench (Fisher, 1954), and the 'Milne-Edwards', 'Krümmel Deep', 'Haeckel Deep' and 'Richards Deep' in the Peru-Chile Trench (Zeigler et al., 1957). The most famous of these 'deeps' is of course the 'Challenger Deep' in the Mariana Trench because it is the deepest area in the world, however, there are also two others nearby in the same trench; the Sirena and Nero Deeps (Fryer et al., 2002).

It is worth noting that the issue of coining 'deeps' has been contentious. In the early 1950s, the British National Committee on Ocean Bottom Features concluded that 'deeps' that were defined from a morphological point of view were relatively unimportant and newly discovered 'deeps' should remain unnamed (Wiseman and Ovey, 1954). The British Committee even omitted 'deeps' from their recognised names of undersea features. The concept of naming 'deeps' is spurred by the desire to declare a new find and does not really offer anything useful scientifically (Wiseman and Ovey, 1954). In fact, in the case where there is a significant 'deep', such as the Mariana Trench, this tends to result in a disproportionate amount of research effort focused on the deepest area thus omitting the rest of the often large trench ecosystem.

4.3. Seafloor heterogeneity

The bathymetric expression of faulting within underriding plates at subduction zone trenches has been reported from the Aleutian (Masson, 1991), Izu-Bonin (Oakley et al., 2008), Japan (Boston et al., 2014), Mariana (Oakley et al., 2008; Emry et al., 2014), Middle America (Ranero et al., 2003) and Peru-Chile (Atacama) (von Huene et al., 1996) trenches, providing strong evidence of bend-related faulting (e.g. Ranero et al., 2003; Oakley et al., 2008). The surface expression of these faults are observed 120 km seaward of the trench axis in Japan Trench (Boston et al., 2014), 100 km seaward of the trench axes of both the Mariana and Izu-Bonin trenches (Oakley et al., 2008), and 60 km seaward of the trench axis in the Middle America Trench (Ranero et al., 2003). This is comparable with the width of faulting observed within the Mariana and Kermadec trenches (100 and 55 km respectively) in this study. Within some subduction zones faults observed cropping out on the seafloor continue to mantle depths (Ranero et al., 2003) although the complexity of faulting will not be fully reflected in the seafloor morphology as the morphology has been proven to average over several faults (Gulick et al., 2004). Fault throws of up to ~500 m were documented in the Middle America Trench (Ranero et al., 2003), up to ~700 m within the Mariana Trench (Oakley et al., 2008), and up to ~500 m within the Izu-Bonin Trench (Oakley et al., 2008). Overall the pattern observed here is similar to fault development in other trenches although larger fault throws were observed within the Mariana (between 120 and 1000 m) and Kermadec (between 150 and 1200 m) trenches than documented elsewhere; this may be a reflection of better quality bathymetry data available compared to previous studies. Additionally, there is observed within the Kermadec and Mariana trenches a subtle interplay between normal fault development, creating horst and grabens, and pre-existing abyssal hill fabrics which intersect and create a zig-zag pattern evident on the seafloor. This complex pattern is documented in other subduction zones (e.g. Boston et al., 2014) where this interaction indicates trench-parallel faulting controlling early brittle deformation with reactivation of pre-existing structures, such as the abyssal hill fabric. Faults produced through fault bending are thought to play a key role in hydration of the upper mantle and crust promoting percolation and circulation of fluids via the faults (e.g. Ranero et al., 2003).

This pervasive fault network can create both elongate fault escarpments that can be laterally continuous, indeed within the Middle America Trench fault escarpments were traced on the seafloor extending ~50 km with variable throw along strike (Ranero et al., 2003) with comparable examples also observed within the Mariana Trench (Emry et al., 2014), and irregular fault paths comprising sharp bends as documented in the Japan Trench (Boston et al., 2014). These not only form troughs, or basins, which can become infilled by sediment, but also form steeply sloping escarpments where hard substrates crop out. Near-vertical, vertical and overhanging cliffs in deep-sea canyons, have been shown to provide the perfect substrate for cold-water coral-based communities (Huvenne et al., 2011). Therefore it can be assumed that escarpments within trench interiors will also provide not only a habitat for sessile marine fauna but also protection from disturbance from mass flow deposits and excessive sedimentation. Mass flows will vary in intensity and frequency such that some may cause community extinction but others may enhance food delivery to the lower reaches of the trench and stimulate benthic activity (Jamieson, 2015).

Seamounts are widely documented as biodiversity hotspots with high levels of endemism (e.g. Clark et al., 2010; Rowden et al., 2005) and typically create elevated currents due to their positive topography resulting in increased local food supply, erosion and deposition of sediments, and often have areas of exposed hard substrate (Clark et al., 2010). Volcanic arcs are the result of subduction process creating seamounts and smaller groups of pinnacles (e.g. Fig. 6c). These pinnacle groups have been observed elsewhere and termed 'petite spot' volcanoes (e.g. Japan Trench (Boston et al., 2014)). Furthermore, seamount chains (e.g. Louisville Seamount Chain) created by intra-plate hot-spot activity are also subducted (e.g. Timm et al., 2013). In addition, they can be subjected to bend-related faulting (e.g. Fig. 5B) and host a variety of substrates and local topographic variability.

It is expected that the local diversity of megafauna increases with an increasing range of substrate types (Taylor and Wilson, 2003). The presence of seamounts, pinnacles, escarpments and sedimentary basins in all three study areas will greatly influence benthic communities due to variability in substrate types observed at local scales (~10 s m; Figs. S2-S4). Where no variety in substrate types was observed at abyssal depths, diversity was recorded as much lower than areas comprising highly sporadic hard substrate habitats for example (Lacharité and Metaxas, 2017). Terrain heterogeneity makes the seafloor of trenches a complex environment to sample, indeed characterising the habitat of associated benthic communities remains challenging due to the limited field of view of cameras and the paucity of sample points within the hadal zone.

4.4. Likelihood of successful seafloor sediment sample recovery

Taking into account this newly realised variability in seafloor topography and substrate the likelihood of successful recovery of a physical sample from hadal areas can be broadly considered. Areas of bedrock cropping out at seabed (e.g. Fig. 8A, C and F), could only be sampled using rotary coring systems. Either a remotely operated seabed rockdrill can be used to obtain short cores from the seabed, or drillships such as the International Ocean Discovery Program (IODP) *Chikyu* or *JOIDES Resolution* can be used to recover longer cores from kilometres sub-seabed. The operation of drillships is expensive for modest research projects and is often only an option open to scientists participating in IODP or indeed in collaboration with industry.

The technical challenges of weight and length of wire-out leads to issues with combined power-lift umbilical cables as well as developing technologies able to operate in high hydrostatic pressure environments prohibits the use of seabed rockdrills within hadal areas. Currently most seabed rockdrills can generally only be deployed to 5500 m water depth (Pheasant et al., 2015). It should be noted however that industry have achieved a 4.4 m rock core sample from 5815 m water depth on the Ueda Ridge, Ogasawara Plateau, which cuts across the southern Izu-Bonin Trench (operations were undertaken on behalf of the Agency for Natural Resources and Energy of Japan in 2006).

It should be acknowledged that the presence of cobbles and pebbles, and a rubbly seafloor, such as has been observed within the Kermadec and Mariana trenches (e.g. Fig. 8B and K), would easily block drill bits used in both rotary coring and vibrocoring. Areas of seafloor comprising gravels (e.g. Fig. 8D, E and I) would also be unlikely to be sampled using sediment corers such as vibrocorers, gravity corers and piston corers. Additionally, significant slope angles (generally > 10°) (e.g. Fig. 6C, G and H) would mean that a seabed rockdrill would be unable to land on the seafloor although this will vary depending on the slope compensation methods installed on individual systems.

This study has highlighted local topographic variability found within hadal areas which was hitherto largely unexplored that would form a hazard to successful deployment of seafloor coring devices even if the issues with operating hadal depths were overcome. Areas of uniform, soft seafloor sediment (e.g. Fig. 8J and L) would likely be successfully sampled using soft sediment corers including maxi- or mega-corers, box-corers, and push cores acquired using Remotely Operated Vehicles. Recent technological advances have seen vibrocorers adapted to operate at water depths up to 6000 m (Stewart, 2015). However these soft-sediment sampling methods continue to rely on the vessels winch cable. Thus far only free-fall lander systems designed to be completely divorced from the vessel have the capability to routinely acquire physical samples from hadal water depths.

5. Conclusions and future direction

The study demonstrates for the first time the high habitat heterogeneity present in hadal zones, across multiple scales. It also serves as a reference to assist future hadal studies as this study has shown that it is perhaps folly to assume that when operating in water depths > 6000 m there is a guarantee of successful recovery of multidisciplinary samples as a result of substrate heterogeneity on multiple, often vastly differing scales. Selecting a trench(es) for study depends largely on the research undertaken, as well as sampling opportunity and vessel logistics. For example, for piezophilic adaptation studies the deepest > 10,000 m trenches are best suited, whereas community structure studies would look to compare populations from trenches of a similar area and depth with different levels of POC flux. Other studies regarding bathymetric and geographic isolation are best targeted with trench communities from different biogeochemical provinces (Table 4) and selected from contrasting isolation clusters derived from Tables 2 and S1. The more statistically robust datasets would be derived from combinations of multiple trenches spanning the four. To provide a practical guide for trench selection, 19 subduction trenches (Aleutian, Atacama, Banda, Bougainville, Izu-Bonin, Java, Kermadec, Mariana, New Britain, New Hebrides, Palau, Philippine, Puerto-Rico, Ryukyu, San Cristobal, South Sandwich, Tonga, Volcano and Yap) are listed in Table 5 against geographic isolation cluster, total trench POC flux (g C yr-1), depth and habitat area.

The development of remotely operated vehicles and automated underwater vehicles with capability to operate at these water depths would revolutionise hadal exploration and tease out relationships between fine-scale heterogeneity and broader-scale studies for better understanding and improved management of our marine environment. The following main conclusions emerge from the research results presented here:

Table 5
Depth (m), Area (km^{-2}) Total Trench POC flux ($g\,C\,yr^{-1}$) and isolation cluster for 19 trenches were all data are available, provided for augmented trench sampling locations.

Trench	Depth (m)	Area (km^{-2})	Total Trench POC flux ($g\,C\,yr^{-1}$)	Isolation Cluster
Aleutian	7669	63,036	1827.27	4
Atacama	7999	26,415	997.24	2
Banda	7329	9963	160.46	5
Bougainville	9103	7423	79.43	5
Izu-Bonin	9701	99,801	1595.41	5
Java	7290	22,689	252.45	5
Kermadec	10,177	49,733	1270.33	5
Mariana	10,984	79,956	606.59	5
New Britain	8844	11,135	110.29	5
New Hebrides	7156	2439	18.15	5
Palau	8021	1692	11.51	5
Philippine	10,540	54,198	395.12	5
Puerto-Rico	8526	52,992	505.09	2
Ryukyu	7531	14,652	145.05	5
San Cristobal	8641	9576	37.15	5
South Sandwich	8125	31,293	384.57	1
Tonga	10,800	65,817	711.16	5

(1) The 47 hadal zones statistically grouped into five significant clusters based on how geographically distant each hadal area is from all other hadal areas with the largest group comprising hadal areas located in the western Pacific Ocean related to subduction around Pacific Plate.
(2) Of the 27 hadal trenches, there is no correlation between depth and descriptors of size (area and length). Furthermore, there is a linear decrease of habitat area with depth common to all trenches, regardless of whether they are deep (> 10,000 m) or shallower trenches.
(3) Asides from geographic isolation and the diminishing area with depth, there are many other factors to consider when addressing the hadal zone beyond 'exceeding 6000 m' or indeed just 'trenches, trench-faults and troughs' as the interior of a trench, for example, is comprised of several large scale topographies, and potentially contrasting habitats, that should also be considered.
(4) Bathymetry data has allowed the seafloor morphology of these three trenches to be revealed in detail. One of the most conspicuous features of the Kermadec and Mariana trenches are the networks of normal fault scarps cropping out at seabed within the trench axis and the underriding plate. These bend-related faults occur in all subduction zones and allow percolation of water into the oceanic plate. The resultant ridges and troughs form significant topographic variation of up to 1000 m with slope angles of up to 40° locally. The depressions form sedimentary basins which become a focus for sedimentary deposition. Furthermore laterally discontinuous ridges are observed on the overriding plates representing the surface expression of underlying thrust faults. Seamounts and smaller pinnacles may represent petite volcanism are also prevalent throughout the trench systems.
(5) The analysis of currently available seafloor photographs acquired from a lander-derived imaging dataset that spans the full depth range of three hadal trenches (including adjacent slopes); the Mariana, Kermadec and New Hebrides trenches suggests there is no correlation between the eight seabed substrate classifications and water depth, geological setting (overriding plate, underriding plate or trench axis) or between the three trenches.
(6) This study has highlighted local topographic variability and previously unrealised variation in seafloor composition found within hadal areas makes the likelihood of successful retrieval of a seafloor sample unpredictable even if the issues with operating at hadal depths were overcome.
(7) 19 subduction trenches where information on total trench POC flux ($g\,C\,yr^{-1}$), depth, habitat area and geographic isolation is presented

as a tool to aid researchers in selecting trench(es) for study.

(8) Multidisciplinary data acquisition which includes seafloor photography and video, biological and geological sampling, high-resolution bathymetry, ocean bottom seismometers and sub-bottom seismic data are necessary to properly assess the impact of local variation in topography, seabed sediment composition and frequency of disturbance on hadal fauna.

Acknowledgements

This work was funded by the TOTAL Foundation (France) through the projects 'Multi-disciplinary investigations of the deepest scavengers on Earth' (2010–2012) and 'Trench Connection' (2013-2015) awarded to AJJ. The 2014 field work was funded by the HADES-K and HADES-M projects supported by the National Science Foundation (NSF) and the Schmidt Ocean Institute (SOI) respectively. We thank the crew and company of the RV *Kaharoa* (KAH1109, KAH1202, KAH1301 and KAH9010), and NIWA Vessels Management, New Zealand. We also thank the crew and company of the RV *Thomas G. Thompson* (TN309; HADES-K), the RV *Falkor* (FK141109; HADES-M) and the Tokyo University of Marine Science and Technology's Training Vessel *TV Shinyo-Maru* (SY1615). We thank Dr. Tomasz Niedzielski (University of Wrocław, Poland) for his unique GIS insights that started this train of thought. Thanks also to Dr Matteo Ichino of the National Oceanographic Centre (UK) who assisted with the benthic POC estimates. HAS was supported in this research by the British Geological Survey (BGS) Ocean Geoscience Team and publishes with the permission of the Executive Director of the BGS (Natural Environment Research Council). The authors wish to thank the Marine Alliance for Science and Technology Scotland (MASTS) Deep-Sea Forum.

Appendix A. Supplementary material

Supplementary data associated with this article can be found, in the online version, at http://dx.doi.org/10.1016/j.pocean.2018.01.007.

References

Amaro, T., Huvenne, V.A.I., Allcock, A.L., Aslam, T., Davies, J.S., Danovaro, R., De Stigter, H.C., Duineveld, G.C.A., Gambi, C., Gooday, A.J., Gunton, L.M., Hall, R., Howell, K.L., Ingels, J., Kiriakoulakis, K., Kershaw, C.E., Lavaleye, M.S.S., Robert, K., Stewart, H.A., Van Rooij, D., White, M., Wilson, A.M., 2016. The Whittard Canyon – a case study of submarine canyon processes. Prog. Oceanogr. 146, 38–57.

Angel, M.V., 1982. Ocean trench conservation. Environmentalist 2, 1–17.

Arzola, R.G., Wynn, R.B., Lastras, G., Masson, D.G., Weaver, P.P.E., 2008. Sedimentary features and processes in the Nazaré and Setúbal submarine canyons, west Iberian margin. Mar. Geol. 250, 64–88.

Belyaev, G.M., 1989. Deep-Sea Ocean Trenches and Their Fauna. Nauka, Moscow.

Blankenship-Williams, L.E., Levin, L.A., 2009. Living deep: a synopsis of hadal trench ecology. Mar. Technol. Soc. J. 43 (5), 137–143.

Boston, B., Moore, G.F., Nakamura, Y., Kodaira, S., 2014. Outer-rise normal fault development and influence on near-trench décollement propagation along the Japan Trench, off Tohoku. Earth Planets Space 66, 135.

Canals, M., Puig, P., Durrieu de Madron, X., Heussner, S., Palanques, A., Fabres, J., 2006. Flushing submarine canyons. Nature 444, 354–357.

Carter, G.D.O., Huvenne, V.A.I., Gales, J.A., Lo Iacono, C., Marsh, L., Ougier-Simonin, A., Robert, K., Wynn, R.B., 2018. Ongoing evolution of submarine canyon rockwalls; examples from Whittard Canyon, Celtic Margin (NE Atlantic). Prog. Oceanogr (accepted for publishcation).

Clark, M.R., Rowden, A.A., Schlacher, T., Williams, A., Consalvey, M., Stocks, K.I., Rogers, A.D., O'Hara, T.D., White, M., Shank, T.M., Hall-Spencer, J.M., 2010. The ecology of seamounts: structure, function, and human impacts. Ann. Rev. Mar. Sci. 2, 253–278.

Danovaro, R., Aguzzi, J., Fanelli, E., Billet, D., Gjerde, K., Jamieson, A., Ramírez-Llodra, E., Smith, C.R., Snelgrove, P.V.R., Thomsen, L., Van Dover, C.L., 2017. An ecosystem-based approach deep-ocean strategy. Science 355, 452–454.

Danovaro, R., Della Croce, N., Dell'Anno, A., Pusceddu, A., 2003. A depocenter of organic matter at 7800m depth in SE Pacific Ocean. Deep-Sea Res. I 50, 1411–1420.

Danovaro, R., Snelgrove, P.V., Tyler, P., 2014. Challenging the paradigms of deep-sea ecology. Trends Ecol. Evol. 29 (8), 465–475.

De Leo, F.C., Smith, C.R., Rowden, A.A., Bowden, D.A., Clarke, M.R., 2010. Submarine canyons: hotspots of benthic biomass and productivity in the deep sea. Proc. Roy. Soc. London B 277, 2783–2792.

Emery, K.O., 1952. Submarine photography with the benthograph. Sci. Monthly 75, 3–11.

Emery, K.O., Merrill, A.S., Trumbull, J.V.A., 1965. Geology and biology of the sea floor as deduced from simultaneous photographs and samples. Limnol. Oceanogr. 10 (1), 1–21.

Emry, E.L., Wiens, D.A., Garcia-Castellanos, D., 2014. Faulting within the Pacific plate at the Mariana Trench: implications for plate interface coupling and subduction of hydrous minerals. J. Geophys. Res. 119, 3076–3095.

Ersts, P.J., Internet. Geographic Distance Matrix Generator (version 1.2.3). American Museum of Natural History, Centre for Biodiversity and Conservation. Available from http://biodiversityinformatics.amnh.org/open_source/gdmg. Accessed on 2017-3-7 (accessed February 2017).

Ewing, M., Vine, A., Worzel, J.L., 1946. Photography of the ocean bottom. J. Opit Soc. Am. 36, 307–321.

Fernandez-Arcaya, U., Ramirez-Llodra, E., Aguzzi, J., Allcock, A.L., Davies, J.S., Dissanayake, A., Harris, P., Howell, K., Huvenne, V.A.I., Macmillan-Lawler, M., Martín, J., Menot, L., Nizinski, M., Puig, P., Rowden, A.A., Sanchez, F., Van den Beld, I.M.J., 2017. Ecological role of submarine Canyons and need for Canyon conservation: a review. Front. Mar. Sci. 4, 5.

Fisher, R.L., 1954. On the sounding of trenches. Deep-Sea Res. 2, 48–58.

Folk, R.L., 1954. The distinction between grain size and mineral composition in sedimentary rock nomenclature. J. Geol. 62, 344–359.

Fryer, P., Becker, N., Applegate, B., et al., 2002. Why is challenger deep so deep? Earth Planet. Sci. Lett. 211, 259–269.

Fujikura, K., Kojima, S., Tamaki, K., et al., 1999. The deepest chemosynthesis-based community yet discovered from the hadal zone, 7326m deep, in the Japan Trench. Mar. Ecol. Press Series 190, 17–26.

Fujioka, K., Takeuchi, A., Horiuchi, K., et al., 1993. Constrated nature between landward and seaward slopes of the Japan Trench off Miyako, Northern Japan. Proc. JAMSTEC Sympos. Deep-Sea Res. 9, 1–26.

Fujiwara, Y., Dato, C., Masui, N., Fujikura, K., Kojima, S., 2001. Dual symbiosis in the cold-seep thyasirid clam *Maorithyas hadalis* from the hadal zone in the Japan Trench, western Pacific. Mar. Ecol. Prog. Ser. 214, 151–159.

Fujiwara, T., Kodaira, S., No, T., et al., 2011. The 2011 Tohoku-Oki earthquake: displacement reaching the trench axis. Science 334, 1240.

Gage, J.D., 2003. Food inputs, utilization, carbon flow and energetic. In: Tyler, P.A. (Ed.), Ecosystems of the World 28, Ecosystems of the Deep Sea. Elsevier, Amsterdam, pp. 315–382.

Gage, J.D., Tyler, P.A., 1991. Deep-Sea Biology: A natural History of organisms at the Deep-Sea Floor. Cambridge University Press, Cambridge.

Gardner, J.V., Armstrong, A.A., Calder, B.R., Beaudoin, J., 2014. So, how deep is the Mariana Trench? Mar. Geod. 37 (1), 1–13.

Garfield, N., Rago, T.A., Schnebele, K.J., Collins, C.A., 1994. Evidence of a turbidity current in Monterey submarine canyon associated with the 1989 Loma Prieta earthquake. Cont. Shelf Res. 14, 673–686.

Gerringer, M.E., Popp, B.N., Linley, T.D., Jamieson, A.J., Drazen, J.C., 2017. Comparative feeding ecology of hadal fishes through stomach contents and amino acid isotope analysis. Deep-Sea Res. I 121, 110–120.

Glud, R.N., Wenzhöfer, F., Middelboe, M., et al., 2013. High rates of microbial carbon turnover in sediments in the deepest oceanic trench on Earth. Nat. Geosci. 6, 284–288.

Gulick, S.P.S., Bangs, N.L.B., Shipley, T.H., Nakamura, Y., Moore, G., Kuramoto, S., 2004. Three-dimensional architecture of the Nankai accretionary prism's imbricate thrust zone off Cape Muroto, Japan: Prism reconstruction via en echelon thrust propagation. J. Geophys. Res. 109, B02105.

Hahn, J., 1950. Some aspects of deep sea underwater photography. J. Photogr. Soc. Am., Section B 16 (6), 27–29.

Heezen, B.C., Ewing, M., 1952. Turbidity currents and submarine slumps and the 1929 Grand Banks earthquake. Am. J. Sci. 250, 849–878.

Heezen, B.C., Hollister, C.D., 1971. The Face of the Deep. Oxford University Press, Oxford.

Heezen, B.C., Johnson, G.L., 1965. The South Sandwich Trench. Deep-Sea Res. 12, 185–197.

Heezen, B.C., Bunce, E.T., Hersey, J.B., Tharp, M., 1964. Chain and Romanche fracture zones. Deep-Sea Res. 11, 11–33.

Huvenne, V.A.I., Tyler, P.A., Masson, D.G., Fisher, E.H., Hauton, C., Hühnerbach, V., Le Bas, T.P., Wolff, G.A., 2011. A picture on the wall: innovative mapping reveals cold-water coral refuge in submarine canyon. PLoS One 6, e28755.

Itou, M., Matsumura, I., Noriki, S., 2000. A large flux of particulate matter in the deep Japan Trench observed just after the 1994 Sanriku-Oki earthquake. Deep-Sea Res. I 47, 1987–1998.

Jamieson, A.J., 2015. The Hadal Zone. Cambridge University Press, Life in the Deepest Oceans'.

Jamieson, A.J., 2018. A contemporary perspective on hadal science. Deep-Sea Res. II (accepted for publishcation).

Jamieson, A.J., Fujii, T., 2011. Trench connection. Biol. Lett. 7, 641–643.

Jamieson, A.J., Fujii, T., Mayor, D.J., Solan, M., Priede, I.G., 2010. Hadal trenches: the ecology of the deepest places on Earth. Trends Ecol. Evol. 25 (3), 190–197.

Jamieson, A.J., Gebruk, A., Fujii, T., Solan, M., 2011. Functional effects of the hadal sea cucumber *Elpidia atakama* (Holothuroidea, Elasipodida) reflect small scale patterns of resource availability. Mar. Biol. 158 (12), 2695–2703.

Jamieson, A.J., Malkocs, T., Piertney, S.B., Fujii, T., Zhang, Z., 2017. Bioaccumulation of persistent organic pollutants in the deepest ocean fauna. Nat. Ecol. Evol. 1, 0051.

Lacey, N.C., Rowden, A.A., Clarke, M., Kilgallen, N.M., Linley, T.D., Mayor, D.J., Jamieson, A.J., 2016. Community structure and diversity of scavenging amphipods from bathyal to hadal depths in three South Pacific trenches. Deep-Sea Res. I 111, 121–137.

Lacharité, M., Metaxas, A., 2017. Hard substrate in the deep ocean: how sediment features influence epibenthic megafauna on the eastern Canadian margin. Deep-Sea Res. I 126, 50–61.

Lemche, H., Hansen, B., Madsen, F.J., Tendal, O.S., Wolff, T., 1976. Hadal life as analysed from photographs. Videnskabelige Meddelelser Fra Dansk Naturhistorik Forening. 139, 263–336.
Levin, L.A., Baco, A.R., Bowden, D.A., Colaco, A., Cordes, E.E., Cunha, M.R., Demopoulos, A.W.J., Gobin, J., Grupe, B.M., Le, J., Metaxas, A., Netburn, A.N., Rouse, G.W., Thurber, A.R., Tunnicliffe, V., Van Dover, C.L., Vanreusel, A., Watling, L., 2016. Hydrothermal vents and methane seeps: rethinking the sphere of influence. Front. Mar. Sci. 3, 72.
Cousins, N.J., D'Onghia, G., Duineveld, G., Shields, M.A., Sion, L., Tursi, A., 2015. Effects of cold-water corals on fish diversity and density (European continental margin: Arctic, NE Atlantic and Mediterranean Sea): Data from three baited lander systems. Deep-Sea Research Part II: Topical Studies in Oceanography.
Linley, T.D., Stewart, A., McMillan, P., Clark, M., Gerringer, M.E., Drazen, J.C., Fujii, T., Jamieson, A.J., 2017. Bait attending fishes of the abyssal zone and hadal boundary: community structure, functional groups and species distribution in the Kermadec, New Hebrides and Mariana trenches. Deep-Sea Res. I 121, 38–53.
Long, D., 2006. BGS detailed explanation of seabed sediment modified Folk classification. http://ec.europa.eu/maritimeaffairs/emodnet/documents/standards/mesh_geology.pdf) (accessed February 2017).
Longhurst, A., 2007. Ecological Geography of the Sea, second edn. Academic Press, San Diego.
Lutz, M.J., Caldeira, K., Dunbar, R.B., Behrenfeld, M.J., 2007. Seasonal rhythms of net primary production and particulate organic carbon flux to depth describe the efficiency of biological pump in the global ocean. J. Geophys. Res.-Oceans 112, C10.
Masson, D.G., 1991. Fault patterns at outer trench walls. Mar. Geophys. Res. 13, 209–225.
Masson, D.G., Harbitz, C.B., Wynn, R.B., Pedersen, G., Løvholt, F., 2006. Submarine landslides: processes, triggers and hazard prediction. Philos. Trans. Roy. Soc. London A: Math., Phys. Eng. Sci. 364 (1845), 2009–2039.
Mengerink, K.J., Van Dover, C.L., Ardron, J., Baker, M., Escobar-Briones, E., Gjerde, K., Koslow, J.A., Ramirez-Llodra, E., Lara-Lopez, A., Squires, D., Sutton, T., 2014. A call for deep-ocean stewardship. Science 344 (6185), 696–698.
Nunoura, T., Takaki, Y., Hirai, M., Shimamura, S., Makabe, A., Koide, O., Kikuchi, T., Miyazaki, J., Koba, K., Yoshida, N., Sunamura, M., 2015. Hadal biosphere: insight into the microbial ecosystem in the deepest ocean on Earth. Proc. Nat. Acad. Sci. 112 (11), E1230–E1236.
Nozaki, Y., Ohta, Y., 1993. Rapid and frequent trubidite accumulation in the bottom of Izu-Ogasawara Trench: Chemical and radiochemical evidence. Earth Planet. Sci. Lett. 120, 345–360.
Oakley, A.J., Taylor, B., Moore, G.F., 2008. Pacific Plate subduction beneath the central Mariana and Izu-Bonin fore arcs: new insights from an old margin. Geochem. Geophys. Geosyst. 9, Q06003.
Oguri, K., Kawamura, K., Sakaguchi, A., Toyofuku, T., Kasaya, T., Murayama, M., Fujikura, K., Glud, R.N., Kitazato, H., 2013. Hadal disturbance in the Japan Trench induced by the 2011 Tohoku-Oki Earthquake. Sci. Rep. 3, 1915.
Otosaka, S., Noriki, S., 2000. REEs and Mn/Al ratio of settling particles: horizontal transport or particulate material in the northern Japan Trench. Mar. Chem. 72, 329–342.
Pheasant, J.I., Wilson, M., Stewart, H.A., 2015. British Geological Survey remotely operated sea bed rockdrills and vibrocorers: new advances to meet the needs of the scientific community. In: 6th International Workshop on Marine Technology, Cartagena, Spain, 15-17th Sept 2015. International Workshop on Marine Technology, 19-21. Available from http://nora.nerc.ac.uk/512686/ (accessed March 2017).
Pratt, R.M., 1962. The ocean bottom. Science 138, 492–495.
R Development Core Team, 2005. R: A Language and Environment for Statistical Computing, R Foundation for Statistical Computing. Vienna, Austria. doi: 10.1007/978-3-540-74686-7.
Randolph, M., Gourvenec, S., 2011. Offshore Geotechnical Engineering. Spon Press, Abingdon, Oxon, UK.
Ranero, C.R., Phipps Morgan, J., McIntosh, K., Reichert, C., 2003. Bending-related faulting and mantle serpentinisation at the Middle America Trench. Nature 425, 367–373.
Rathburn, A.E., Levin, L.A., Tryon, M., et al., 2009. Geological and biological heterogeneity of the Aleutian margin (1965–4822m). Prog. Oceanogr. 80, 22–50. http://dx.doi.org/10.1016/j.pocean.2008.12.0.
Ritchie, H., Jamieson, A.J., Kilgallen, N.M., Piertney, S.B., 2015. Phylogenetic relationships among hadal amphipods of the Superfamily Lysianassoidea: implications for taxonomic revision and biogeographic distribution. Deep-Sea Res. I 105, 119–131.
Romankevich, E.A., Vetrov, A.A., Peresypkin, V.I., 2009. Organic matter of the World Ocean. Russ. Geol. Geophys. 50, 299–307.
Rowden, A.A., Clark, M.R., Wright, I.C., 2005. Physical characterisation and a biologically focused classification of "seamounts" in the New Zealand region. N. Z. J. Mar. Freshwater Res. 39 (5), 1039–1059.
Ryan, W.B.F., Carbotte, S.M., Coplan, J.O., O'Hara, S., Melkonian, A., Arko, R., Weissel, R.A., Ferrini, V., Goodwillie, A., Nitsche, F., Bonczkowski, J., Zemsky, R., 2009. Global multi-resolution topography synthesis. Geochem., Geophys. Geosyst. 10, Q03014.
Saunders, P.M., 1981. Practical conversion of pressure to depth. J. Phys. Oceanogr. 11, 573–574.
Shimanaga, M., Yanagi, K., 2016. The Ryukyu Trench may function as a "depocenter" for anthropogenic marine litter. J. Oceanogr. 72 (6), 895–903.
Stewart, H.A., 2015. What lies beneath: offshore data acquisition and how we turn those data into science. In: Proceedings of the Open University Geological Society, 1. 23-33. Available to download from http://nora.nerc.ac.uk/510725/ (accessed March 2017).
Tarn, J., Peoples, L.M., Hardy, K., Cameron, J., Bartlett, D.H., 2016. Identification of free-living and particle-associated microbial communities present in hadal regions of the Mariana Trench. Front. Microbiol. 7, 665.
Taylor, P.D., Wilson, M.A., 2003. Paleoecology and evolution of marine hard substrate communities. Earth Sci. Rev. 62, 1–103.
Thistle, D., 2003. The deep-sea floor: an overview. In: Tyler, P.A. (Ed.), Ecosystems of the World 28, Ecosystems of the Deep Sea. Elsevier, Amsterdam, pp. 5–37.
Thornburg, T.M., Kulm, L.D., 1987. Sedimentation in the Chile Trench: depositional morphologies, lithofacies, and stratigraphy. Geol. Soc. Am. Bull. 98, 33–52.
Thunell, R., Tappa, E., Varela, R., et al., 1999. Increased marine sediment suspension and fluxes following an earthquake. Nature 398, 233–236.
Timm, C., Bassett, D., Graham, I.J., Leybourne, M.I., de Ronde, C.E.J., Woodhead, J., Layton-Matthews, D., Watts, A.B., 2013. Louisville seamount subduction and its implication on mantle flow beneath the central Tonga-Kermadec arc. Nat. Commun. 4, 1720.
Turnewitsch, R., Falahat, S., Stehlikova, J., Oguri, K., Glud, R.N., Middleboe, M., Kitazato, H., Wenzhoefer, F., Ando, K., Fujio, S., 2014. Recent sediment dynamics in hadal trenches: evidence for the influence of higher-frequency (tidal, near-inertial) fluid dynamics. Deep-Sea Res. I 90, 125–138.
Tyler, P.A., 1995. Conditions for the existence of life at the deep-sea floor: an update. Oceanogr. Mar. Biol.: Ann. Rev. 33, 221–244.
Tyler, P., Amaro, T., Arzola, R., Cunha, M.R., de Stigter, H., Gooday, A., Huvenne, V., Ingels, J., Kiriakoulakis, K., Lastras, G., Masson, D., Oliveira, A., Pattenden, A., Vanreusel, A., Van Weering, T., Vitorino, J., Witte, U., Wolff, G., 2009. Europe's grand Canyon: Nazaré Submarine Canyon. Oceanography 22, 46–57.
Van Dover, C., 2000. The Ecology of Deep-Sea Hydrothermal Vents. Princeton University Press.
Vetter, E.W., Dayton, P.K., 1998. Macrofaunal communities within and adjacent to a detritus-rich submarine canyon system. Deep-Sea Res. II 45, 25–54.
von Huene, R., Pecher, I.A., Gutscher, M.-A., 1996. Development of the accretionary prism along Peru and material flux after subduction of the Nazca Ridge. Tectonics 15, 19–33.
von Huene, R., Scholl, D.W., 1991. Observations at convergent margins concerning sediment subduction, subduction erosion, and the growth of continental crust. Rev. Geophys. 29, 279–316.
Watling, L., Guinotte, J., Clarke, M.R., Smith, C.R., 2013. A proposed biogeography of the deep ocean floor. Prog. Oceanogr. 111, 91–112.
Webb, T.J., Berghe, E.V., O'Dor, R., 2010. Biodiversity's big wet secret: the global distribution of marine biological records reveals chronic under-exploration of the deep pelagic ocean. PLoS One 5 (8), e10223.
Wentworth, C.K., 1922. A scale of grade and class terms for clastic sediments. J. Geol. 30, 377–392.
Wenzhöfer, F., Oguri, K., Middelboe, M., Turnewitsch, R., Toyofuku, T., Kitazato, H., Glud, R.N., 2016. Benthic carbon mineralization in hadal trenches: Assessment by in situ O_2 microprofile measurements. Deep-Sea Res. Part I: Oceanogr. Res. Papers 116, 276–286.
Wickham, H., Chang, W., 2007. ggplot2: An Implementation of the Grammar of Graphics. GNU General Public License. ⟨https://cran.r-project.org/web/packages/ggplot2⟩. CRAN (accessed February 2017).
Wiseman, J.D.H., Ovey, C.D., 1954. Proposed names of features on the deep-sea floor, 1. The Pacific Ocean. Deep-Sea Res. 2, 93–106.
Wright, D.J., Pendleton, M., Boulware, J., Walbridge, S., Gerlt, B., Eslinger, D., Sampson, D., Huntley, E., 2012. ArcGISBenthic Terrain Modeler (BTM), v. 3.0, Environmental Systems Research Institute, NOAA Coastal Services Center, Massachusetts Office of Coastal Zone Management. Available online at http://esriurl.com/5754.
Yancey, P.H., Gerringer, M.E., Drazen, J.C., Rowden, A.A., Jamieson, A.J., 2014. Marine fish may be biochemically constrained from inhabiting deepest ocean depths. Proc. Natl. Acad. Sci. 111 (12), 4461–4465.
Zeigler, J.M., Athearn, W.D., Small, H., 1957. Profiles across the Peru-Chile Trench. Deep-Sea Res. 4, 238–249.